Air Force Institute of Technology

AFIT Scholar

Theses and Dissertations   Student Graduate Works

3-7-2008

Damage Detection Analysis Using Lamb Waves in Restricted Geometry for Aerospace Applications

Roman T. Underwood

Follow this and additional works at: https://scholar.afit.edu/etd

Part of the Aerospace Engineering Commons

Recommended Citation

Damage Detection Analysis Using Lamb Waves
in Restricted Geometry
for Aerospace Applications

THESIS

Roman T. Underwood, Captain, USAF

AFIT/GAE/ENY/08-M29

DEPARTMENT OF THE AIR FORCE
AIR UNIVERSITY

AIR FORCE INSTITUTE OF TECHNOLOGY

Wright-Patterson Air Force Base, Ohio

AFIT/GAE/ENY/08-M29

Damage Detection Analysis Using Lamb Waves in Restricted Geometry for Aerospace Applications

THESIS

Presented to the Faculty

Department of Aeronautical and Astronautical Engineering

Graduate School of Engineering and Management

Air Force Institute of Technology

Air University

Air Education and Training Command

In Partial Fulfillment of the Requirements for the

Degree of Master of Science in Aeronautical Engineering
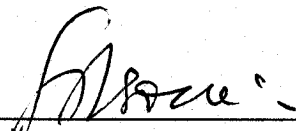
Roman T. Underwood, B.S.

Captain, USAF

March 2008

DAMAGE DETECTION ANALYSIS USING LAMB WAVES
IN RESTRICTED GEOMETRY
FOR AEROSPACE APPLICATIONS

Roman T. Underwood, B.S.

Captain, USAF

Approved:
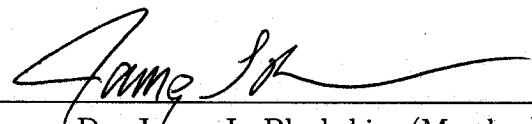
_____

Dr. Som R. Soni (Chairman)

_3/7/08_

date

_____

Maj Eric D. Swenson (Member)

_3/7/08_

date

_____

Dr. James L. Blackshire (Member)

_3/7/08_

date

AFIT/GAE/ENY/08-M29

Abstract

Today many USAF aircraft are approaching the end of their projected service life. However, those aircraft, such as the F-15 Eagle, are still being operated to accomplish the mission of the USAF. As the F-15 ages the required maintenance increases, as does the risk of structural failure. A goal of structural health monitoring (SHM) programs is to increase aircraft safety by monitoring areas known to have structural failures. Currently, time intensive manual inspections are used to monitor failure "hotspots" decreasing the readiness of the F-15 fleet. The lead ziconate titanate (PZT) is a commonly used piezoelectric transducer that has shown the potential to detect damage in aircraft structures without time consuming manual inspections. However, many locations where damage has occurred that have been identified by the USAF for SHM systems have restricted geometries consisting of thickness changes and boundary surfaces located near the damage. The restricted geometry presents challenges when using PZT sensors because of the interference of reflected waves coming off of boundary surfaces, and the behavior of the signals going through thickness changes. For this research, a location has failed on multiple F-15 aircraft and has been selected as a basis to evaluate some of the challenges of using PZT sensors for SHM. The goal of this research is to detect fatigue cracks in plates that represent the restricted geometry of the aircraft bulkhead so as to determine if a real damage detection system could be built for F-15 bulkheads. This research shows that detecting closed fatigue cracks can be more challenging than detecting cracks opened by a static load, but applying static loads present new challenges.

Acknowledgements

I would like to acknowledge the Dayton Area Graduate Studies Institute (DAGSI) and the Air Force Research Lab (AFRL) for their support of this research. I need to thank my advisor Dr. Som Soni, and committee members Maj Eric Swenson and Dr. James Blackshire for their expertise and assistance in all aspects this thesis. I would also like to acknowledge Mr. Mark Derriso (AFRL), Dr. Martin DeSimio (ATK Mission Research), and Dr. Steven Olson (University of Dayton Research Institute) for their suggestions, encouragement, and expert help throughout this experiment. Also, I would like to thank Mr. Todd Bussey (AFRL) for his assistance in verifying the experimental setup and data collection system. Finally I would like to thank Mr. Jay Anderson (Air Force Institute of Technology) and his team for their expertise in material and mechanical experimental test setup.

Roman T. Underwood

Table of Contents

List of Figures

x

List of Tables

List of Symbols

List of Abbreviations

Damage Detection Analysis Using Lamb Waves in Restricted Geometry for Aerospace Applications

I. Introduction

1.1 Motivation

The "health" of an aircraft determines its overall readiness and its ability to perform a required mission. Therefore, knowledge of an aircraft's structural health is essential in maintaining fleet readiness. Typically, the depot performs structural health assessments and compiles the structural health information to estimate the structural health of the fleet, but with the advances of structural health monitoring (SHM) systems, it may be possible for field-level maintainers to regularly monitor an aircraft's structural health. Field-level knowledge of aircraft structural health can be used to determine when depot-level maintenance of an aircraft is necessary. If we can know when an aircraft needs to be serviced - a.k.a. condition based maintenance - as opposed to servicing at a fixed interval, we could increase aircraft readiness while decreasing sustainment costs [5].

The United States Air Force (USAF) has aircraft with internal support structures, known as bulkheads, known to suffer from fatigue cracks. The bulkheads identified by the USAF have complex and restrictive geometries, see Figure 1.1. Because the aircraft must be disassembled in order to access the bulkhead shown, lengthy inspection times are required to check for damage. The aircraft systems known to suffer from these identified fatigue cracks are forced to endure the lengthy inspections to ensure the operational safety of the aircraft, which means the readiness of the these aircraft is reduced. An attached SHM system installed at bulkhead locations of known fatigue cracks could reduce the lengthy inspection times, increasing the readiness of the aircraft and reporting the structural health of the aircraft.

1

Figure 1.1:   USAF aircraft bulkhead known to suffer fatigue cracks [7]

1.1.1   Nondestructive Evaluation (NDE).   Monitoring the structural health of an aircraft is any important part of maintenance [12]. Today, structural health monitoring is usually accomplished through programmed depot-level maintenance. Structural health inspections can also be conducted at the field-level, but such an inspection requires lengthy and labor intensive disassembly procedures. Both depot-level and field-level structural health inspections create down time for an aircraft system, but the losses in readiness are made up in increases in safety and reliability. NDE of an aircraft offers a solution to lengthy, and potentially destructive, disassembly inspections. NDE can be accomplished through nondestructive inspections (NDI) or through SHM systems. The difference between NDI and SHM is the state of the system when the inspection occurs. NDI inspections occur while the aircraft is offline, basically set aside for maintenance [5]. SHM can occur while the system is online, and is a non-intrusive inspection by nature [5].

1.1.1.1   NDI/SHM Techniques.   Some current NDI methods used by the USAF are eddy current, fluorescent penetrant, magnetic particle, radiography, and ultrasonic testing [4], which are described next. Eddy current testing is used on materials that conduct electricity where a magnetic field is used to induce a current through the material. The current levels are measured to determine if the structure

is damaged [1]. Eddy current testing is a good method for detecting small cracks, but requires skilled personnel, access to the desired test location, and can only be used on materials that conduct electricity [1].

Fluorescent penetrant testing uses a fluorescent chemical to seep into discontinuities and an ultraviolet lamp excites the fluorescent penetrant, allowing damage to be visually detected [4]. Fluorescent penetrant testing is dependent on the the ability of the penetrant to enter a discontinuity, and the material it is trying to penetrate [4].

The magnetic particle test involves applying an electrical current to a ferromagnetic part, thus magnetizing it [4]. Discontinuities in the part creates poles, and when magnetic particles are introduced to the magnetized part, they are attracted to the poles [4]. Once again, a drawback to magnetic particle testing is the requirement to have access to the part.

Radiography testing uses electromagnetic radiation to test the interior of structural objects. Radiography testing detects damage by identifying localized changes in the object's composition and density-thickness product [4]. Disadvantages of radiography testing are that it requires access to the area to be tested, and radiography is a radiation hazard to the personnel assigned to perform the inspection.

Ultrasonic testing utilizes piezoelectric transducers set up in an array to generate and measure elastic waves in the structure being inspected [4]. A disadvantage of the current method for using piezoelectric transducers for NDI is the need to calibrate the transducer array to the structure to be tested. To calibrate the piezoelectric transducer array, a model of the structure is produced with simulated damage [4]. The measurements taken on the structure from piezoelectric transducer array is compared to the measurements taken on the model.

Ultrasonic testing has shown the potential to be used in SHM systems, but it is not commonly used in the fleet. Piezoelectric transducers can be permanently attached to an aircraft structure, and wired to a maintenance surface port. The transducers can then be either excited by an onboard system or by a technician

during routine maintenance, eliminating the need for lengthy disassemblies to access the structure for each inspection.

1.2 Research Objectives

The lead ziconate titanate (PZT) is a commonly used piezoelectric transducer, which can be bonded to the surface of a structure to generate Lamb waves in material [11]. The PZT is considered a smart material because it is capable of both sensing and actuating signals [5]. Using this principal, we explore using PZTs in a "pitch-catch" approach, where Lamb waves are created (pitched) by one PZT and received (caught) by another, to detect cracks in a solid piece of aluminum. Previous research and experimentation by Swenson and Crider [15] using Lamb waves to detect damage in a simulated aircraft bulkhead used notches to simulate damage. This research effort extends their work by using real cracks in a test article that represents the restricted geometry in a bulkhead, because an actual aircraft bulkhead could not be used.

This thesis accomplishes the objectives of the research by reviewing the relevant theory, Chapter 2, applied during experimentation and analysis, then discussing the setup and conducting of the experiments, Chapter 3. Chapter 4 presents the results of each experiment, and finally Chapter 5 discusses the conclusions of the experiment results and suggests topics for future research.

II. Background Theory

This chapter discusses theories important to this thesis research. The primary theories are wave and piezoelectric theory. Wave theory is important to this thesis research because it discusses the theory and property of Lamb waves which are important in both the experimental setup and the analysis of the experimental results. Piezoelectric theory is reviewed to discuss the theory of the piezoelectric properties of the sensors used in the experiment.

2.1   Wave Theory

Mechanical waves are elastic disturbances created by the restoring forces of the elastic medium [14]. The basic wave equations are:

$$\frac{\partial^2 \phi}{\partial x^2} + \frac{\partial^2 \phi}{\partial y^2} + \frac{\omega^2}{c_L^2}\phi = 0 \tag{2.1}$$

$$\frac{\partial^2 \psi}{\partial x^2} + \frac{\partial^2 \psi}{\partial y^2} + \frac{\omega^2}{c_T^2}\psi = 0 \tag{2.2}$$

Where ϕ and ψ are potential functions, and c_L, c_T are the longitudinal and transverse wave speeds respectively, and x and y are coordinates in the plane of motion. The longitudinal wave speed and transverse wave speed are defined as:

$$c_L = \sqrt{\frac{\lambda + 2\mu}{\rho}} \tag{2.3}$$

$$c_T = \sqrt{\frac{\mu}{\rho}} \tag{2.4}$$

where ρ is the density; λ and μ are Lamé constants [13]. Lamé constants are:

$$\mu = \frac{E}{2(1+\nu)} \tag{2.5}$$

$$\lambda = \frac{E\nu}{(1-2\nu)(1+\nu)} \tag{2.6}$$

5

where E is the Young's modulus and ν is Poisson's ratio. The general solutions to Equations (2.1) and (2.2) are:

$$\phi = [A_1 sin(py) + A_2 cos(py)]e^{i(kx-\omega t)} \tag{2.7}$$

$$\psi = [B_1 sin(qy) + B_2 cos(qy)]e^{i(kx-\omega t)} \tag{2.8}$$

In Equations (2.7) and (2.8) x is the coordinate in the wave propagation direction, y is the coordinate in the direction of plate thickness, and k is the Lamb wave number defined as:

$$k = \frac{2\pi}{L} \tag{2.9}$$

where L is the wavelength. Likewise, p and q from (2.7) and (2.8) are defined as:

$$p = \sqrt{\frac{\omega^2}{c_L^2} - k^2} \tag{2.10}$$

$$q = \sqrt{\frac{\omega^2}{c_T^2} - k^2} \tag{2.11}$$

Boundary conditions are used solve for A_1, A_2, B_1, and B_2 in Equations (2.7) and (2.8), and for thin plates, the dispersion equations for Lamb waves are:

$$\frac{tan(\frac{qd}{2})}{tan(\frac{pd}{2})} = -\frac{4k^2 pq}{(q^2 - k^2)^2} \tag{2.12}$$

$$\frac{tan(\frac{qd}{2})}{tan(\frac{pd}{2})} = -\frac{(q^2 - k^2)^2}{4k^2 pq} \tag{2.13}$$

where d is the thickness of the plate. The Equations (2.12) and (2.13) describe the two most common types of Lamb waves: symmetrical (S), and anti-symmetrical (A). There are many solutions to the Lamb wave equations corresponding to the Lamb wave number (k) resulting in many Lamb wave modes $(S_0, S_1, S_2, \ldots$, and $A_0, A_1, A_2, \ldots)$.

The Lamb wave mode defines the properties of the Lamb wave in the material. In an elastic plate, the symmetric modes of Lamb waves cause particles of the plate to move in opposite directions of the thickness of the plate, see Figure 2.1(a). The antisymmetric modes of Lamb waves cause the particles of the plate to move in the same direction, relative to each other, through the thickness of the plate, see Figure 2.1(b) [16].
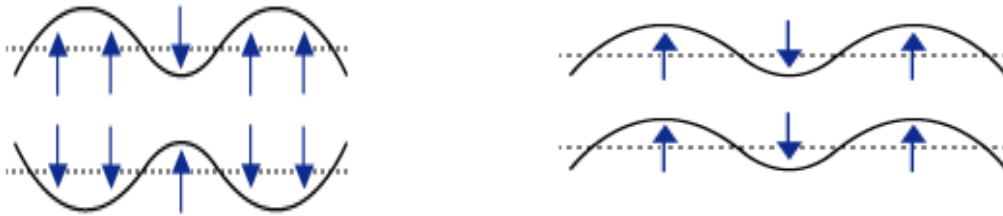
(a) Symmetric wave form.   (b) Antisymmetric wave form.

Figure 2.1:   Examples of plate particle displacement during Lamb wave modes [2].

Lamb waves traveling through a material, such as aluminum, have wave speeds that are dependent upon their frequency [6]. This is because aluminum is a dispersive medium [14]. Where Lamb waves experience dispersion, defined as the temporal increase in the extent of the signal, the dispersive wave speed, also known as the phase velocity, v_p, can be predicted by [14].:

$$v_p = \frac{\omega}{k} \tag{2.14}$$

where $\omega = 2f\pi$ and f is the frequency in Hz. The phase velocity is the speed at which the peaks of the wave move along the length of the plate in the direction of wave propagation [7]. However, since a packet excites energy over a wide range of frequencies, an additional velocity needs to be defined to characterize the velocity

of the packet [14]. Therefore, the group velocity, v_g, of the excited waves can be considered the velocity of the excitation signal, which is predicted by:

$$v_g = \frac{d\omega}{dk} \tag{2.15}$$

Computing the group velocity allows us to estimate the time of arrival (TOA) of each wave packet at the primary excitation frequency see Figure 2.2.
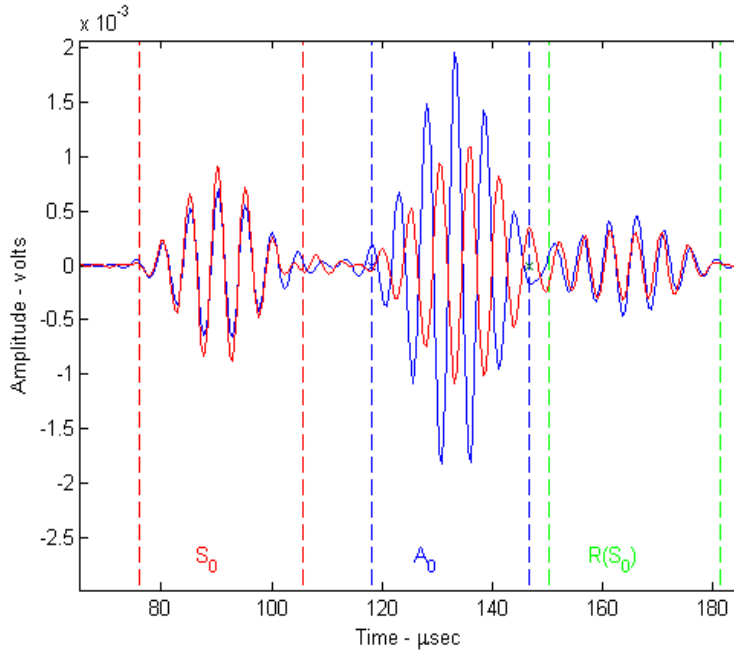
Figure 2.2:   Predicted windows based on estimate of packet group velocity, v_g.

The phase and group velocities, are not only dependent on the frequency of excitation but are also a function of the thickness of the plate. For this study, the thickness is constant - a similar thickness as the F-15 bulkhead - throughout all the experiments, therefore the phase and group velocities can be thought of as only function of frequency in this study. Also, the thickness of the plates used in this research and the excitation frequency range is such that only the first fundamental frequency of the symmetric and antisymmetric, S_0 and A_0 respectively, modes are excited in the structure.

8

Giurgiutiu, see Figure 2.3, indicates the response amplitude of the A_0 wave is larger at frequencies between 50 and 270 kHz [10]. Likewise the S_0 response amplitudes are larger at frequencies above 270 kHz [10]. During the excitation, the mode expected to produce the best return at the excitation frequency will be used to collected data to detect damage. By selecting the appropriate frequency and corresponding Lamb wave mode window, S_0 or A_0, to detect damage is known as tuning [10]. Tuning is a useful technique for measuring response because specific waveforms are targeted, and reflected wave amplitudes can be minimized.
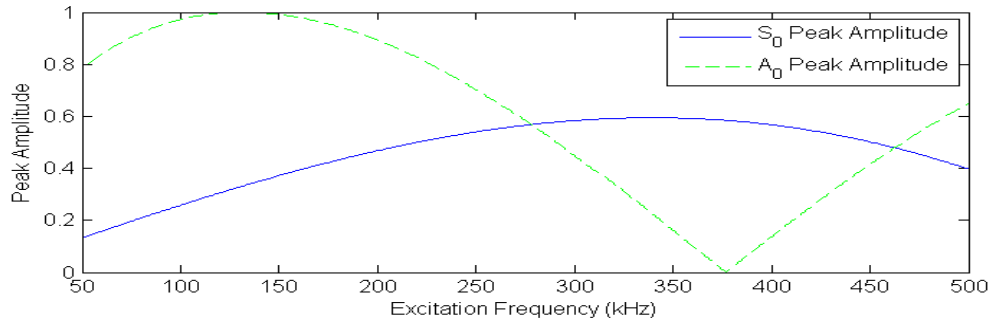
Figure 2.3: Theoretical normalized amplitude of the S_0 and A_0 Lamb wave modes for excitation frequencies 50 to 500 kHz in a 3 mm thick plate [10].

2.2 Piezoelectric Properties

In 1880, Jacques and Pierre Curie discovered the piezoelectric effect [3]. The piezoelectric effect is the phenomenon of mechanical strain applied to a material producing a proportional electrical field. The reverse is also true, known as the inverse piezoelectric effect, that an electric field applied to a material produces proportional mechanical strain [3]. The generalized constitutive equations relating mechanical strain and the electrical field of a piezoelectric material is given by:

$$S_{ij} = s^E_{ijkl}T_{kl} + d_{kij}E_k \tag{2.16}$$

$$D_j = d_{jkl}T_{kl} + \varepsilon^T_{jk}E_k \tag{2.17}$$

E is the Young's modulus, S_{ij} is the mechanical strain, T_{kl} is the mechanical stress, E_k is the electrical field, D_j is the electrical displacement, s_{ijkl} is the mechanical compliance of the material at zero electrical field, ε_{jk}^T is the dielectric permittivity measured at zero mechanical stress, and d_{kij} is the coupling between electrical and mechanical variables [9].

PZT wafers, like shown in Figure 2.4, are constructed with positively charged metal ions, such as titanium, and negatively charged ions, such as lead, mixed in powder form with oxygen molecules in specific proportions. Under the appropriate conditions the mixed powder is heated and then combined with a binder to form the desired shape.
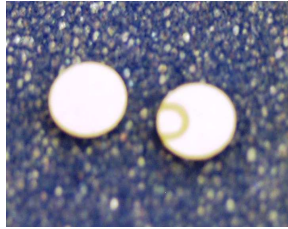
Figure 2.4:   Top and bottom of PZT discs used in this research.

Many materials have been found to possess piezoelectric properties, but the most popular material is lead zirconate titanate (PZT). PZT is cost effective to produce and has higher operating temperatures and greater sensitivity than other piezoelectric materials [3]. PZTs are considered a smart material - meaning they are capable of both actuating and measuring signals [5].

For damage detection, the typical approaches are the "pulse-echo" method and the "pitch-catch" method. The "pulse-echo" method uses one PZT sensor to excite a signal then the same PZT to measure the returning reflected signal (known as the "echo") [7]. Damage is detected by predicting the expected time of flight (TOF) of the echo response in a healthy structure and determining the TOF window of the echo response in a potentially damaged structure. The "pitch-catch" method excites (pitches) one PZT then measures (catches) the response at another PZT [7].

Damage is detected by comparing the amplitude of the measured healthy responses to responses after damage is suspected to have occurred. If damage has occurred, the measured response can have decreased amplitude and/or a phase shift.

III.   Experimental Setup

This chapter discusses the set-up and methodology used for the two experiments of this research; the Large Flat Plate (LFP) and bulkhead-webbing crack detection experiments. The purpose of the LFP experiment is to validate the window estimation code for using PZT sensors to generate Lamb waves in an aluminum test specimen. The goal of the bulkhead-webbing experiment is to detect a closed crack in restricted geometry, similar to what would be seen in the F-15 bulkhead webbing.

3.1   Equipment

The primary equipment used in all of our experiments, shown in Figure 3.1, includes an Agilent 33120A arbitrary waveform generator, a Hewlett Packard 54621A oscilloscope, and a National Instruments PCI-6133 data acquisition card (DAQ) set up to sample at 2.5 MHz while recording up to eight signals simultaneously. The Agilent waveform generator is used to create a 5.5 cycle Hanning-windowed sine wave, see Figure 3.2, at a variety of frequencies, and the LabVIEW® software controls the excitation and measurement of the response signals.

The PZT actuators are excited over the frequency range 50 to 500 kHz in 10 kHz increments. We constructed a voltage divider to divide the excitation amplitude by 1,000 before it enters the connector block to minimize induction in the connector block. The PZT sensors are American Piezo Ceramics (APC) 850, 6.35 mm diameter discs and are bonded to the surface of the test plate using M-Bond 200 Adhesive. The PZT sensors are connected with shielded coaxial cables to the waveform generator and connector block.

3.1.1   TOA Windows.   The phase and group velocity of each waveform, at the excitation frequency, is used to predict the time of arrival (TOA) windows for the S_0 and A_0 waveform packets. The arrival times for the direct S_0 and A_0 packets are based on the location of the PZT sensors. Taking the plate geometry into consideration we are also able to predict the TOA windows for the first reflection of

Figure 3.1:   Data collection system.
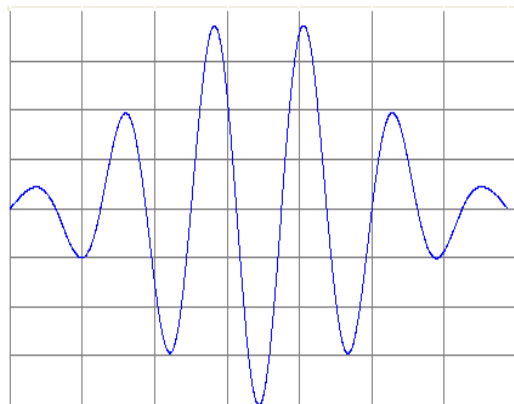
Figure 3.2:   5.5 cycle Hanning-windowed sine wave.

the S_0 waveform. Because the predicted TOA windows of the first reflection of the A_0 waveform is always after the TOA of the first reflection of the S_0 waveform in our experiments, we only consider the first reflection of the S_0 packet.

3.2 Large Flat Plate Experiment

The first step to using PZT sensors to detect damage is to characterize the behavior of PZT generated Lamb waves in our aluminum sample. Titanium is used to make some aircraft bulkheads, but Titanium is difficult to work with and expensive. Aluminum is a suitable replacement for titanium because the Lamb wave group velocities in aluminum are similar to the Lamb wave group velocities in titanium. We attach four PZT sensors to a 24 in x 48 in x 1/8 in thick aluminum test plate. PZT sensors 1 and 2 are attached 287 mm apart on the front of the plate, as shown in Figure 3.3. The separation distance is designed to maximize the separation of arrival times between the direct S_0 packet, the direct A_0 packet, and the first reflections of each packet. PZT sensors 3 and 4 are atteched directly opposite PZT sensors 1 and 2, respectively, on the back of the plate. A pitch-catch approach is used with all four PZT sensors to excite and measure Lamb wave responses and experiment with mode isolation both in excitation and measurement.

The LFP experiment has four phases. First, exciting at one PZT and measuring the response at one PZT, such as exciting at PZT 1 and measuring at PZT 2. The next phase is to excite two PZTs, front and back, simultaneously while measuring the response at one PZT, such as exciting PZTs 1 and 3 and measuring PZT 2. By exciting from two PZTs front and back simultaneously, one can theoretically cancel out the anti-symmetric waveform, creating only the symmetric waveform. The third phase is to excite two PZTs, front and back, simultaneously as before except the back PZT (PZT 3 or 4) will be excited 180 degrees out of phase. By exciting the back PZT out of phase, one can theoretically cancel out the symmetric waveform, creating only the anti-symmetric waveform. The final phase of the LFP experiment is to excite one PZT and measure the response from two PZTs, front and back, simultaneously, such
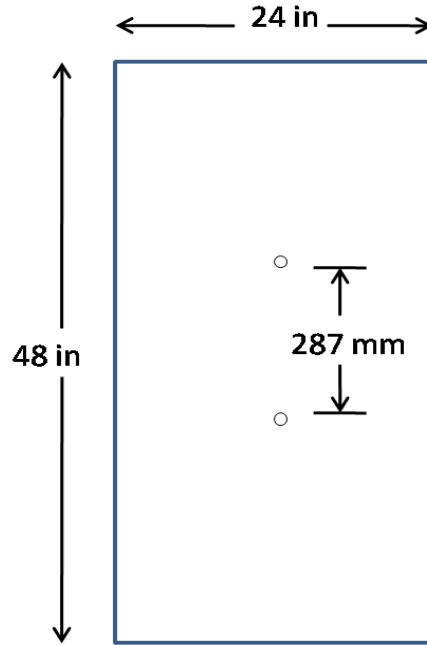
Figure 3.3:   LFP set-up.

as exciting PZT 1 and measure PZTs 2 and 4. When the responses from PZTs on the front and back are compared they should be in phase during the symmetric waveform and 180 degrees out of phase during the anti-symmetric waveform.

In the LFP experiment we designed the sensor placement, 287 mm apart, to separate the predicted arrival's of each waveform and their first reflections. Figure 3.4 shows the predicted arrival and departure times of each packet. This gives us a good opportunity to identify waveforms without the interference of reflections or simultaneous direct arrivals.

The LFP experiment allows us to gage our ability to predict the size and location of the TOA windows for the direct S_0, direct A_0, and the first reflected S_0 waveform packets. By attaching sensors on both the front and back of plate we we are theoretically able to isolate the S_0 and A_0 waveforms by either exciting two PZTs simultaneously or measuring responses at two PZTs simultaneously. Once we identify each waveform we should be confident that:

15
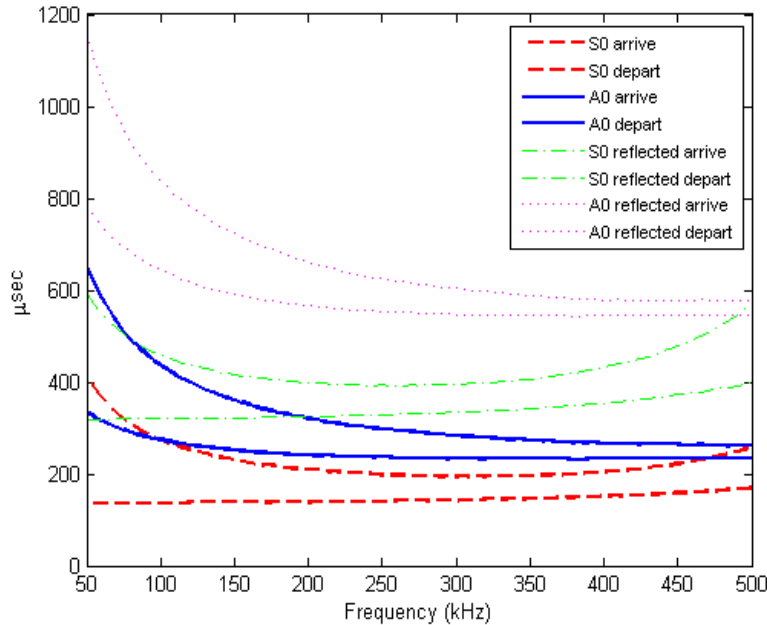
Figure 3.4:   LFP waveform arrival and departure times based
on 287mm sensor separation.

1. we are producing Lamb waves because we see both symmetric and anti-symmetric
   waveforms and

2. we can accurately predict TOA windows for direct and reflected Lamb wave
   packets.

3.3   Bulkhead-Webbing Crack Experiment

We then machined several test plates out of the aluminum sheet used for the
LFP experiment to begin the bulkhead-webbing crack detection experiment. We
cut the bulkhead-webbing test plates out of the aluminum sheet used for the LFP
experiment so that we know we are able to accurately predict the TOA windows and
the frequencies where the response should be dominated by the S_0 or A_0 packet. The
test plates are "dogbone" shaped test coupons with an overall test area of 80 mm
x 120 mm, which represents the dimensions of an actual aircraft bulkhead webbing
(see Figure 3.5(a)). The top and bottom rows of PZTs are only 40 mm apart, which

16

represents the expected placement of the PZTs on the F-15 bulkhead. A total of
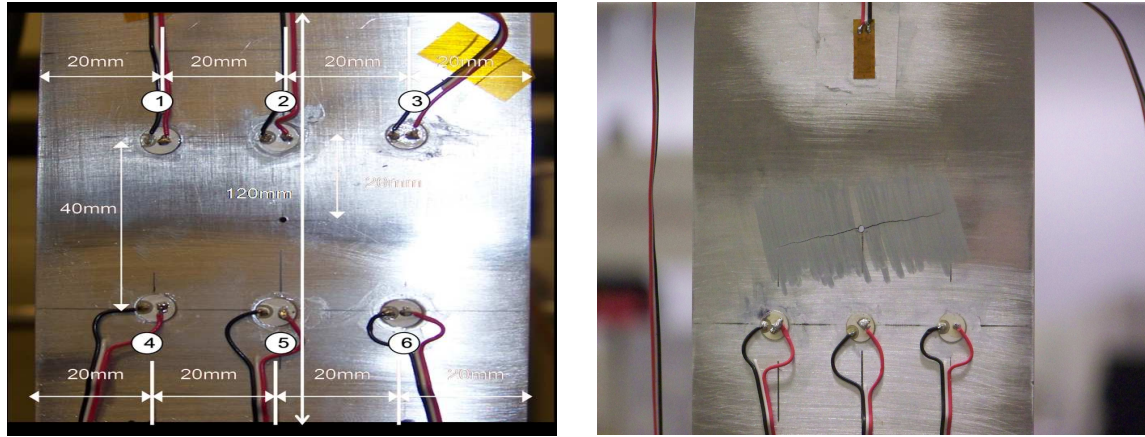
(a) Front of the bulkhead-webbing test plate(undamaged)

(b) Back of the bulkhead-webbing test plate (damaged)

Figure 3.5: PZT configuration on Bulkhead-Webbing test plate.

nine PZTs are attached to the test plate, six on the front side and three on the back. Additionally, there is a CEA-06-25OUN-350 standard strain gage, rated to 5,000 μstrain, located on the back of the plate (see Figure 3.5(b)). To detect damage, we use a pitch-catch approach where PZTs 1, 2, and 3, as shown in Figure 3.5(a), are the actuators that create the Lamb waves and PZTs 4, 5, 6, and PZTs 4B, 5B, and 6B, as shown in Figures 3.5(a) and 3.5(b) respectively, are used to sense the Lamb waves. PZTs 4B, 5B, and 6B are located directly opposite PZTs 4, 5, and 6 on the back of the test plate. PZTs 1, 2, and 3 are centered on the plate with 20 mm of separation (measured center to center) between each other and from the edge of the plate. PZTs 4, 5, and 6 are horizontally lined up with PZTs 1, 2, and 3. The two rows are evenly spaced, 20 mm from the center of the test area, where the crack propagates.

The restricted geometry of aircraft bulkheads presents challenges in using PZT sensors. The row of actuating PZTs (1, 2, and 3) is located 40 mm from the row of measurement PZTs (4, 5, 6, 4B, 5B, and 6B), making the separation time between the direct S_0 and first reflected S_0 packet arrives for vertical PZT pairs 1-4, and 3-6 approximately 4 μs. For most of the PZT pairs, during the bulk or our excitation frequency range, the TOA of the first reflection occurs before the end of both the

17

direct S_0 and direct A_0 packets, as shown in Figure 3.6(a). Therefore, the S_0 TOF window is reduced in length to exclude the first reflected S_0 mode, as shown in Figure 3.6(b). This is particularly important when reflected waves could propagate along a path that takes them around damage, and therefore lead to false negative indications of damage [5]. However, we do not reduce the A_0 TOF window because the S_0 mode amplitude is significantly lower than the A_0 mode between 50 and 200 kHz.
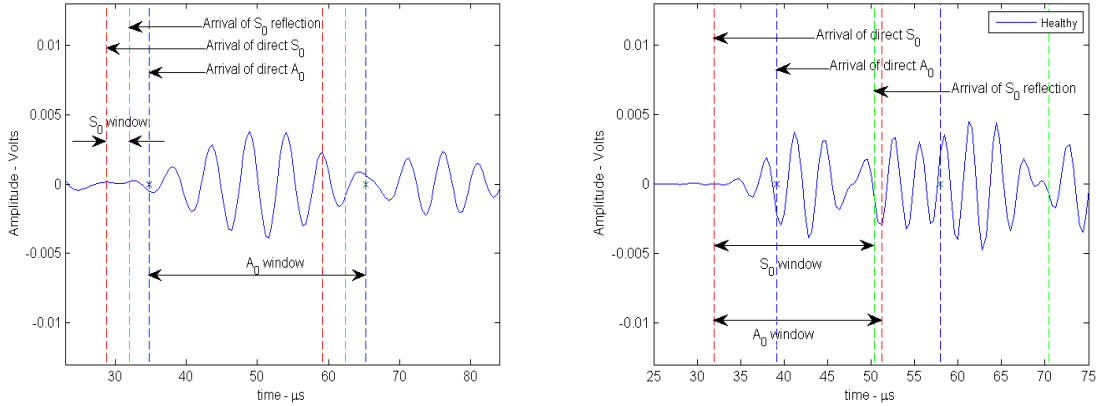
(a) Small S_0 window while exciting PZT 2 and measuring PZT 6 at 180 kHz

(b) Large S_0 window while exciting PZT 2 and measuring PZT 6 at 180 kHz

Figure 3.6: Size of S_0 and A_0 windows during Bulkhead-webbing experiment.

A 1.67 mm hole, simulating a rivet hole, is drilled into the center of the test area of each plate. Cyclic loading is applied by a 110 kip hydraulic test machine (810 Material Test System). The load schedule to propagate fatigue cracks is experimentally determined on a test plate without PZTs attached. To detect damage, we excite PZTs 1, 2, and 3 in turn while collecting responses at PZTs 4, 4B, 5, 5B, 6, and 6B simultaneously. We load the plate to 100 lbs to collect data, which prevents the plate from going into compression while still maintaining a closed crack. A x10 telescopic lens is used to measure the horizontal length of the crack to an accuracy of 1/100 of a mm. The crack is measured horizontally from left to right and includes the diameter of the simulated rivet hole.

IV. Experiment Results

The goal of this thesis is to determine if PZT sensors can be used to detect a propagated fatigue crack with Lamb waves in restricted geometry representative of an actual F-15 bulkhead. To accomplish this task, Lamb wave characterization was done on a large flat plate made of 6061-T6 aluminum. Then, test plates, cut from the same sheet of aluminum as the large flat plate are cyclicly loaded to propagate fatigue cracks in them. The results from both experiments are discussed in this chapter.

4.1   Analysis Techniques

Three types of analysis techniques are used in this thesis. The first technique evaluates the PZT responses in the time domain. This technique is useful when predicting the TOA windows and evaluating potential interference of overlapping of wave packets. Another technique used in this thesis is to compare the amplitude of the responses in a healthy plate to the amplitude of responses after damage occurs. The amplitude of the response is defined as:

$$S_0 response = \sqrt{\sum_{i=t_a}^{t_b} x_i^2} \tag{4.1}$$

$$A_0 response = \sqrt{\sum_{i=t_c}^{t_d} x_i^2} \tag{4.2}$$

where t_a is the arrival time of the direct S_0 mode, t_b is the arrival time of the first S_0 reflection or the predicted end of the direct S_0 packet (whichever is predicted to arrive first), t_c is the arrival time of the direct A_0 mode, and t_d is the predicted end of the A_0 packet. The response calculations are repeated at every frequency in the excitation range, and the response amplitudes are plotted against frequency. The third type of analysis in this thesis is to plot the response amplitudes against the number of fatigue cycles. Plotting against fatigue cycles displays trends in the PZT responses after having been subjected to fatigue loading.

4.2   LFP Results

Lamb waves have certain characteristic behaviors, as mentioned in Chapter 2, and the goal of the LFP experiment is to determine if we can accurately predict TOA windows and isolate modes for application in the next experiment. The PZTs are attached on the sheet of aluminum such that during most frequencies in our excitation range, the direct S_0, direct A_0, and reflected S_0 waves arrive and depart without overlapping each other. The windowing technique allows us to capture only the response data occurring at the expected TOA of each waveform; we want to verify our ability to predict the TOA windows for each mode packet in this experiment. Figure 4.1 shows the mode packets in our predicted windows (dashed verticel lines).
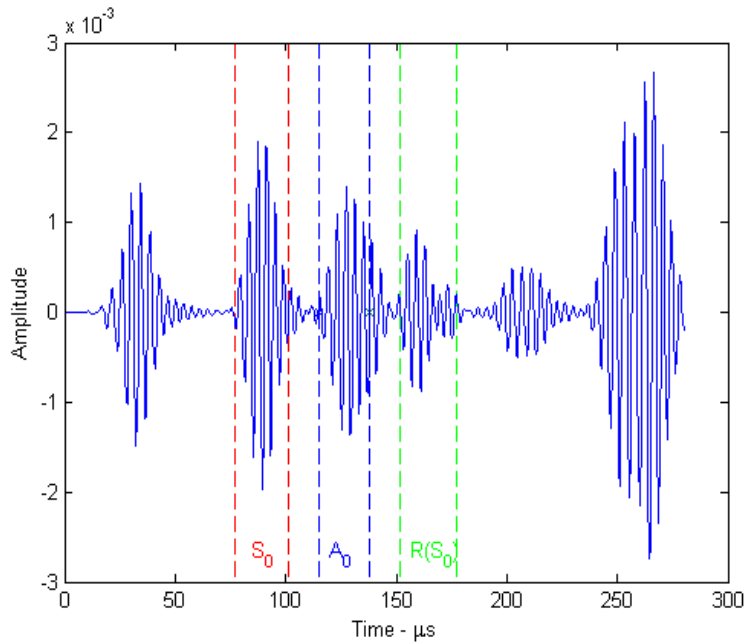
Figure 4.1:   Lamb waves in expected TOA windows for LFP experiment, 240 kHz excitation frequency at PZT 1, measured at PZT 2.

Figure 4.1 displays characteristic results of phase one of the LFP experiment. The S_0 waveform packet is enclosed in the predicted S_0 window, as is the A_0 waveform packet and the predicted first reflected S_0 waveform packet. Phase two, three, and four of the LFP experiment are designed to identify the waveform packets by isolating

either the S_0 or the A_0 waveform. Phase two of the LFP experiment is to excite two PZTs, located front-to-back with each other, simultaneously to cancel out the A_0 mode. First we excited PZTs 2 and 4 and measured at PZT 1. Figure 4.2 shows that with 450 kHz excitation signal the A_0 waveform response is effectively canceled out. Comparing Figure 4.2 to Figure 4.3 the decrease in A_0 amplitude is evidence the dual excitation canceled out the A_0 mode. However, at 210 kHz, (Figure 4.4) exciting at two PZTs simultaneously did not cancel out the A_0 waveform, as seen by the amplitude in the A_0 window. Unfortunately Figure 4.4 displays the trend, not the exception, when isolating the S_0 waveform by exciting at two PZTs simultaneously. The A_0 waveform is greater in amplitude than the S_0 waveform between 50 and 200 kHz, and without having the PZTs exactly opposite each other not enough of the waveform packet is canceled out. Exciting two PZTs, front-to-back, is not a reliable technique for damage detection, and no further research is conducted in this area.
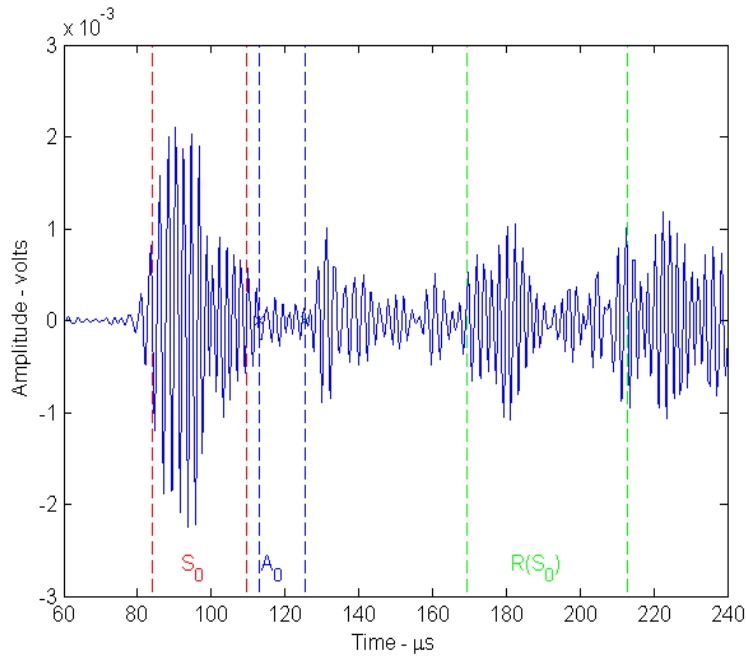

Figure 4.2: Responses of the S_0 waveform by exciting PZTs 2 and 4 simultaneously in phase at 450 kHz.
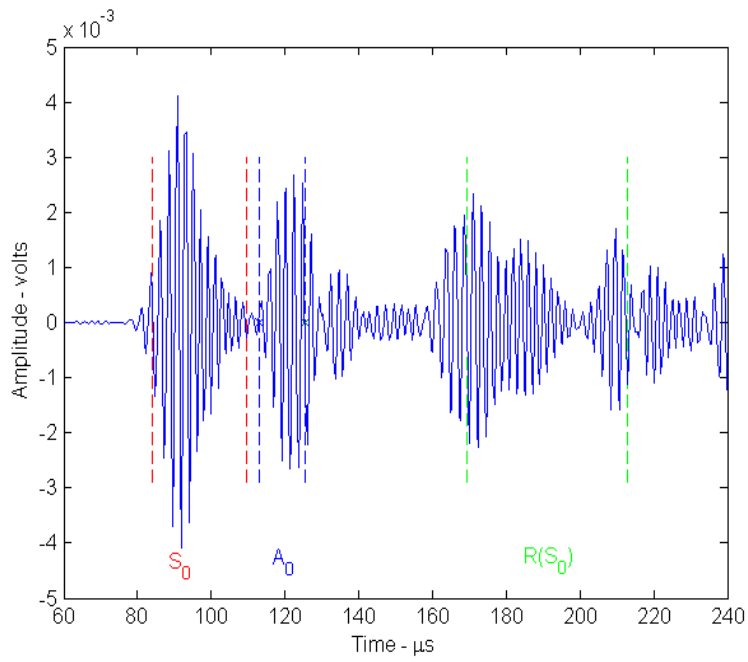
Figure 4.3: Responses of the S_0 and A_0 waveforms exciting PZT 2 and measuring PZT 1 at 450 kHz.
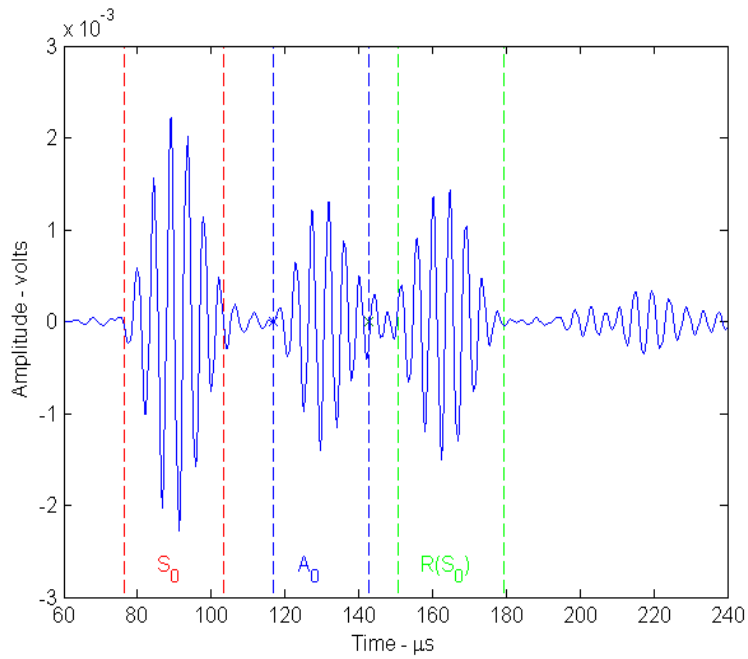

Figure 4.4: Response of the S_0 and A_0 modes by exciting PZTs 2 and 4 simultaneously in phase at 210 kHz

In the next phase of the LFP experiment, we attempt to isolate the A_0 mode by exciting two PZTs, front-to-back with respect to each other, 180 degrees out of phase. Figure 4.5 shows the S_0 mode packet effectively minimized, when compared to Figure 4.6, by exciting PZTs 2 and 4 at 190 kHz, 180 degrees out of phase with respect each other. The expected A_0 response amplitude is larger than the expected S_0 response amplitude at 190 kHz excitation frequency, however after 220 kHz the expected S_0 response amplitude is larger than the expected A_0 response amplitude, and Figure 4.7 shows the S_0 packet is not being canceled out by the dual excitation. Exciting two PZTs, front-to-back, 180 degrees out of phase with respect to each other is not a reliable technique for damage detection, and no further research is conducted in this area.
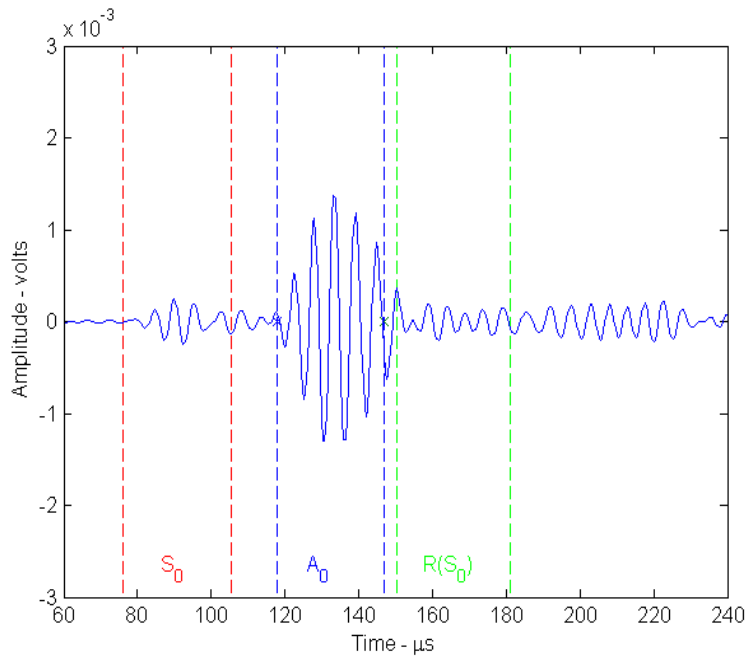
Figure 4.5:   Isolated A_0 waveform by exciting PZTs 2 and 4 simultaneously out of phase at 190 kHz

Phase four the LFP experiment is to isolate the S_0 and A_0 modes by measuring at two PZTs, front-to-back, simultaneously. The time response of the measurement PZTs overlayed with each other show the S_0 packets are in phase, and the A_0 packets are 180 degrees out of phase, as shown in Figure 4.8. The difference in response

23
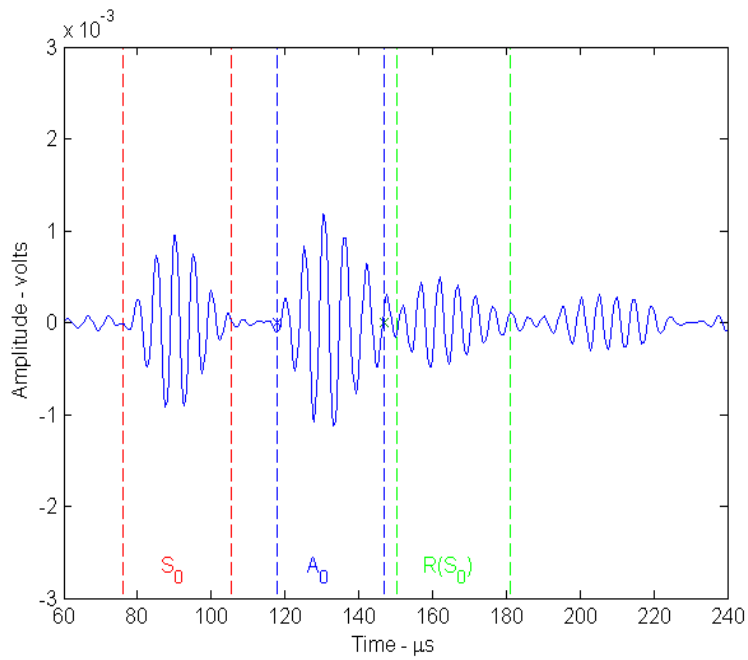
Figure 4.6:   Responses of the S_0 and A_0 waveforms exciting PZT 2 and measuring PZT 1 at 190 kHz.
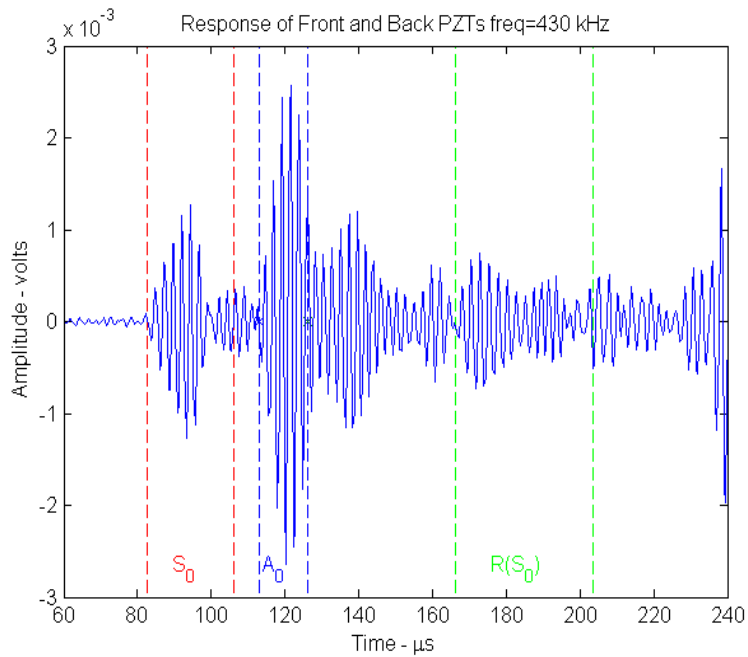
Figure 4.7:   Isolated S_0 waveform by exciting PZTs 2 and 4 simultaneously out of phase at 430 kHz

24

amplitude between the two PZTs can be attributed to a gain, or natural amplitude, difference in the individual PZTs.
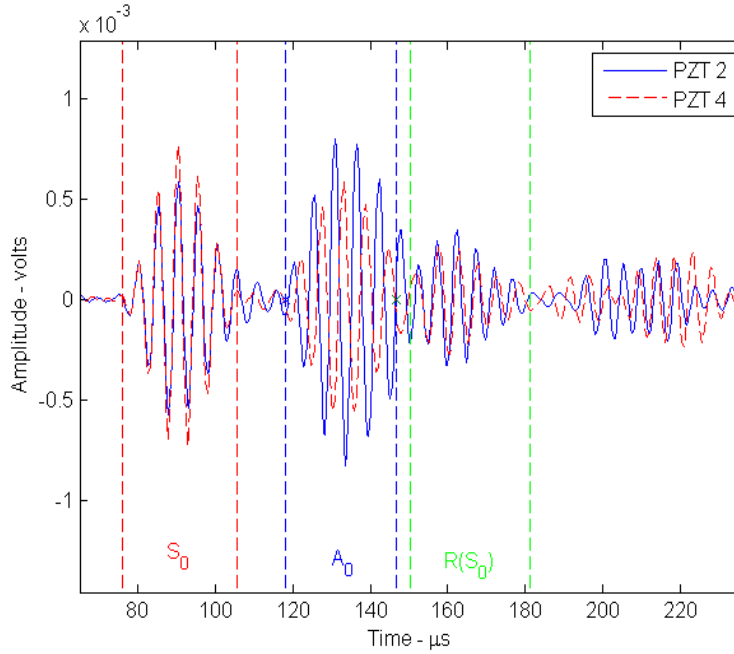
Figure 4.8:   Front and back sensor measurements displaying mode types.

Figures 4.1 and 4.8 show that we are able to clearly identify the S_0 and A_0 waveforms correctly and accurately. The next step is to generate Lamb waves in a realistic geometry, similar to the F-15 bulkhead, and detect fatigue cracks.

4.3   Bulkhead-Webbing Crack Results

Five test plates cut from the aluminum sample are used in LFP experiment with a water jet cutting table for the bulkhead-webbing crack experiment. The five plates have identical geometries, where the test region of the test plate has similar dimensions as the webbing of the F-15 bulkhead. The first two plates were used to experimentally develop a loading schedule/method capable of propagating a 30 mm crack in a timely manner. The third plate was instrumented with PZT sensors and a strain gage, but a crack developed at a stress concentration point outside of the test area and the plate failed shortly after cyclic loading began. The final two plates,

referred to as test plates 4 & 5, were instrumented and successfully propagated cracks of at least 29 mm in length. The results of those experiments are discussed here.

Since we use a "pitch-catch" approach to detect damage in the plate, PZT pairs and wave propagation paths are selected that minimize the interference of the first reflected S_0 mode and increase the probability of crack detection. The path between PZT pairs 2-5 and 2-5B include the rivet hole (see Figure 4.9, and therefore once a crack is present, the propagation path between PZTs 2-5 and 2-5B is always completely interrupted by the fatigue crack. Conversely, the paths between PZT pairs 1-4, 1-4B, 3-6, and 3-6B are the farthest from the rivet hole, and are never completely interrupted by the crack. The data from the paths between 1-4, 1-4B, 2-5, 2-5B, 3-6, and 3-6B can be used as a control to better understand the effects of continued fatigue loading on the PZTs. Figure 4.9 shows the PZT pairs that have propagation paths interrupted by the growing crack. It is the paths between these PZT pairs where we look for decreases in the response amplitude due to damage.
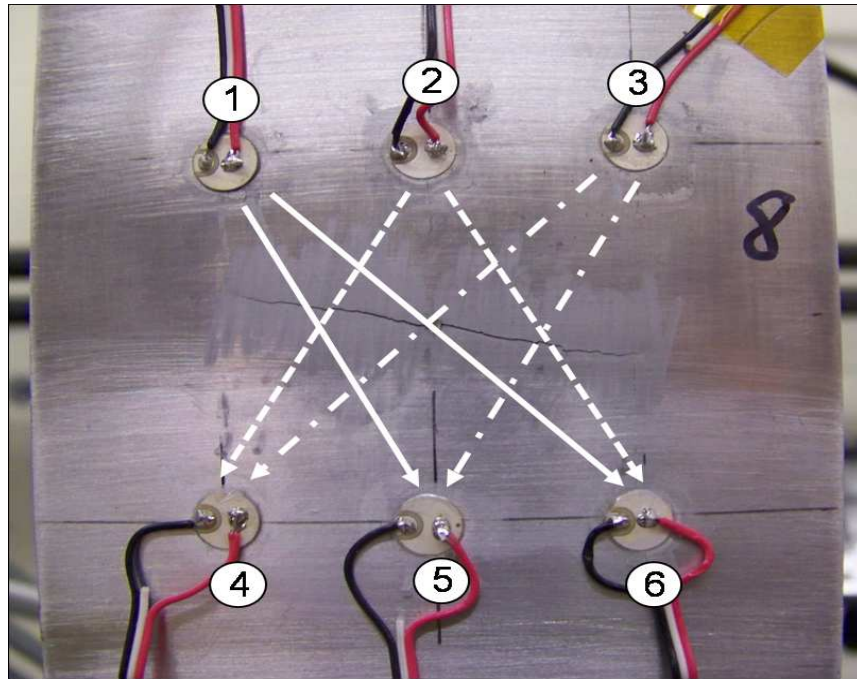

Figure 4.9:   Bulkhead-webbing PZT setup with wave propagation paths indicated (shown with 36 mm crack).

4.3.1   Test Plate 4.   To accomplish the goal of this research, cyclic loads are applied to the test plate with a 110 kip MTS hydraulic test machine, as shown in Figure 4.10. The loading schedule used to grow a crack to various lengths was previously determined on test plates of similar geometry and listed in Table 4.1. The applied loads resulted in a maximum stress of 79% of the yield stress for 6061-T6 aluminum [8] in the bulk of the plate, but exceeded yield at the simulated rivet hole causing damage to the plate. The loads shown in Table 4.1 are not necessarily representative of actual loading that an aircraft bulkhead would experience in flight or on the ground, but were selected to grow a crack in a timely manner. Before propagating fatigue cracks in the test plate, data is collected to form a baseline of healthy responses under a nominal 100 lb static loading. This small static load is used keep the plate under tension, preventing any accidental compressive loading.
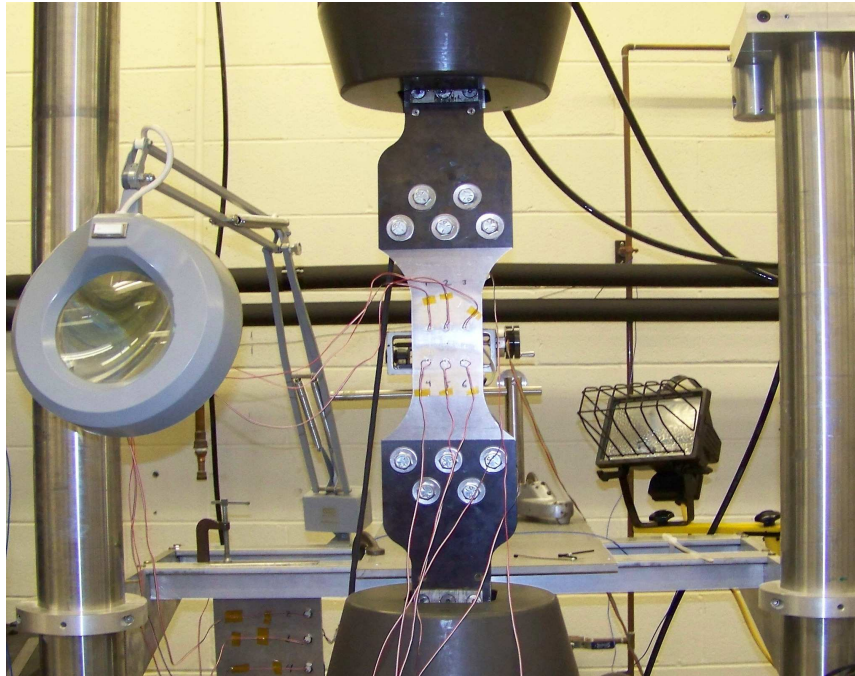

Figure 4.10:   Test plate shown in MTS machine for cyclic loading.

4.3.1.1   Plate 4, 1st Crack Increment.   After 12,000 loading cycles, a through-crack was visually observed in the test plate emanating from both sides of the

27

Table 4.1:   Loading schedule and crack length for test plate 4.

Cyclic Loading		
Load(kips)	Cycles	Crack Length(mm)
13 - 1.3	12,000	7.61*
10 - 1.0	2,000	8.57*
9 - 0.9	2,000	9.07
9 - 0.9	2,000	9.65
10 - 1.0	2,000	16.47*
8 - 0.8	2,000	16.79
9 - 0.9	1,518	21.38*
8 - 0.8	1,000	22.85
8 - 0.8	1,000	26.21*
6 - 0.6	4,000	26.71
7 - 0.7	1,800	29.55*

* data collected

simulated rivet hole. Data is collected and analyzed using Equations (4.1) and (4.2), and variation in the response amplitude at all six PZT sensors when excited from each of the three actuator PZTs was observed. The variation in response amplitude is dependent on the excitation frequency, showing a decrease at many frequencies but an increase at some frequencies. Figure 4.11 shows a decrease in response amplitude in the A_0 and S_0 (200 - 400 kHz) windows from the healthy baseline to the first crack length from PZT 1 to PZT 5. There is also an amplitude decrease in both the A_0 and S_0 windows from PZT 2 to PZT 4, Figure 4.12. Since the crack is 7.61 mm long, it does not intersect the propagation paths of the PZT pairs 1-5 and 2-4, shown in Figures 4.11 and 4.12, therefore there should not be a decrease in response amplitude.

When the plate was loaded to 13 kips, the strain in the bulk of the plate was approximately 3,300 μstrain. According to Kusaka, a surface mounted PZT will decrease in amplitude after several loading cycles exceeding 3,000 μstrain [11]. This may account for the difference in response amplitude of the PZT pairs without a crack intersecting the wave propagation path. This could indicate the PZTs have been degraded by the cyclic loading.
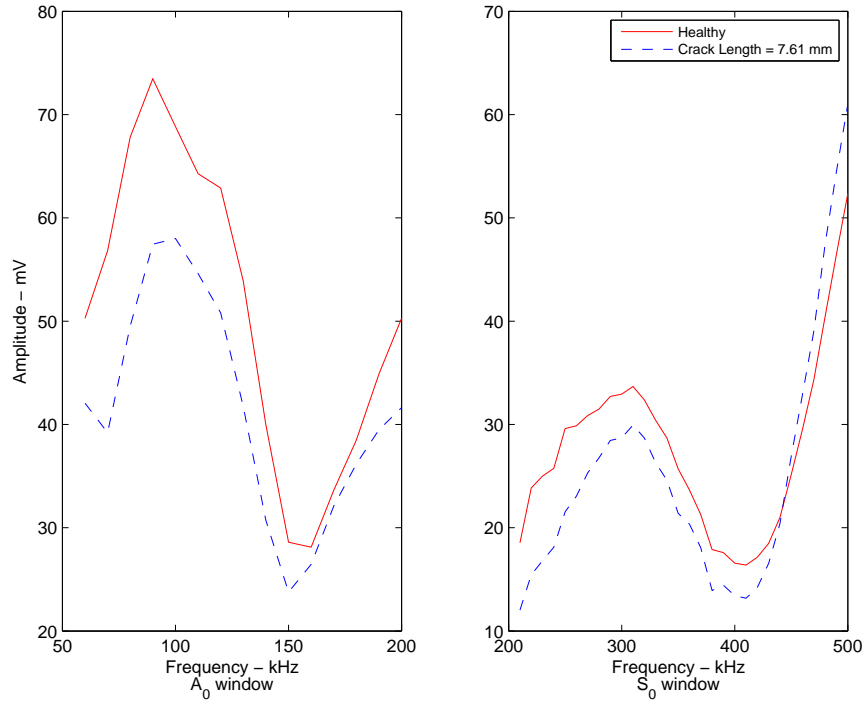
Figure 4.11: A_0 and S_0 response when exciting PZT 1, measuring PZT 5 with 7.61mm crack in Plate 4.
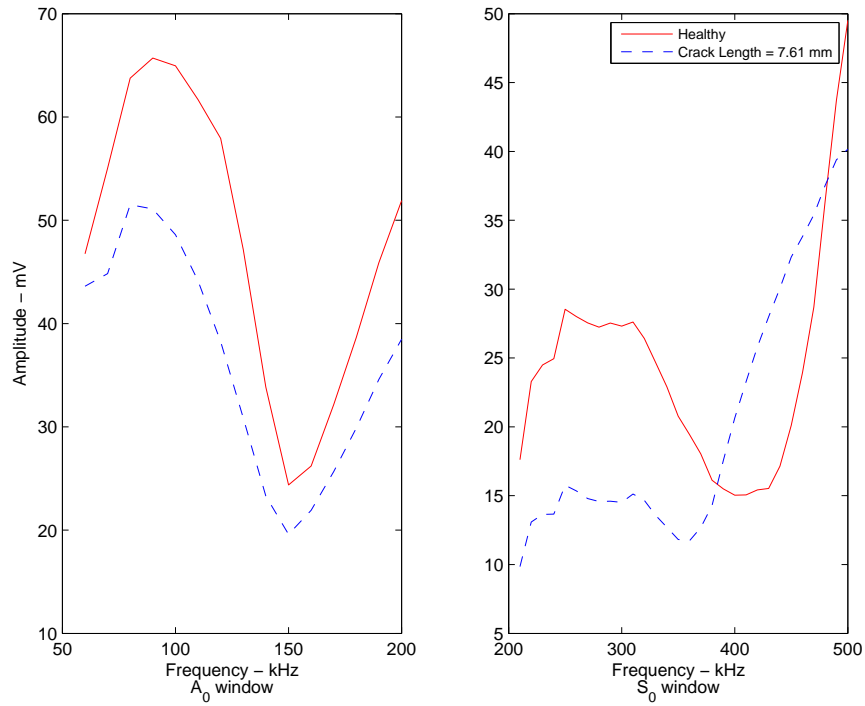

Figure 4.12:   Frequency response exciting PZT 2, measuring PZT 4 with 7.61 mm crack in Plate 4.

4.3.1.2 Plate 4, 2nd Crack Increment. After 2,000 more cycles, responses are collected at a crack length of 8.57 mm. The crack still does not intersect the propagation path between PZT pairs 1-5, 1-5B, 2-4, 2-4B, 2-6, 2-6B, 3-5, and 3-5B, therefore their responses should not show a decrease in amplitude when compared to the response amplitude measured after the first crack length. Figures 4.13 and 4.14 show the responses of the PZT pairs 1-5 and 3-5B respectively. As can be seen there is very little change in the response amplitude measured in either the A_0 or S_0 windows after a 7.61 mm crack to the response amplitude measured at a 8.57 mm crack. This correctly indicates no damage has occurred in the propagation paths of these PZT pairs.

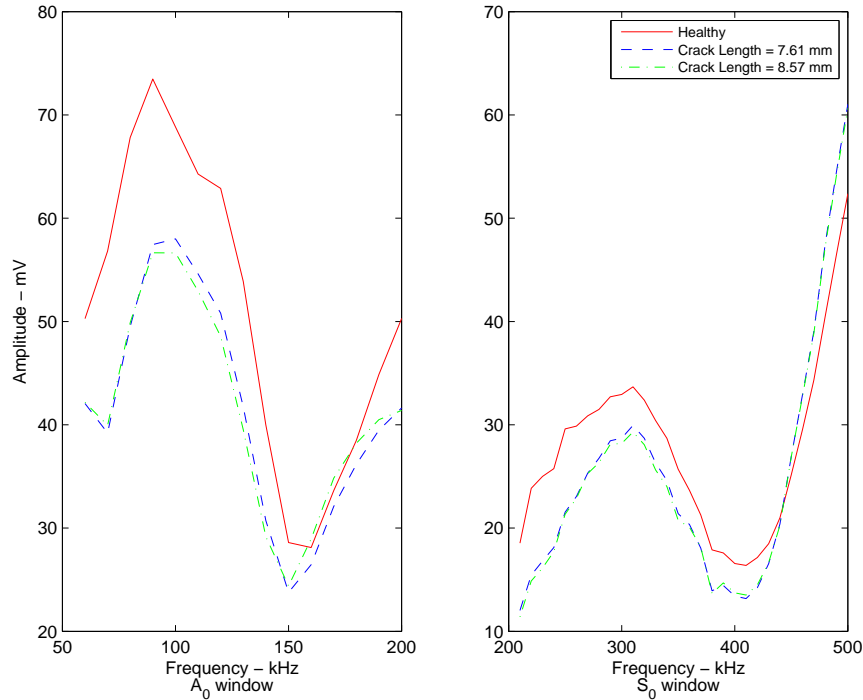Figure 4.13: Response exciting PZT 1, measuring PZT 5 in Plate 4 with respect to excitation frequency.

4.3.1.3 Plate 4, 3rd Crack Increment. Data was collected at a crack length of 16.47 mm. PZT pairs such as 1-6 and 3-4 have a relatively long propagation path compared to the path of PZTs 2-6, ect. The propagation paths of PZT pairs 1-6 and 3-4 also include the rivet hole, but the relatively long propagation path allows
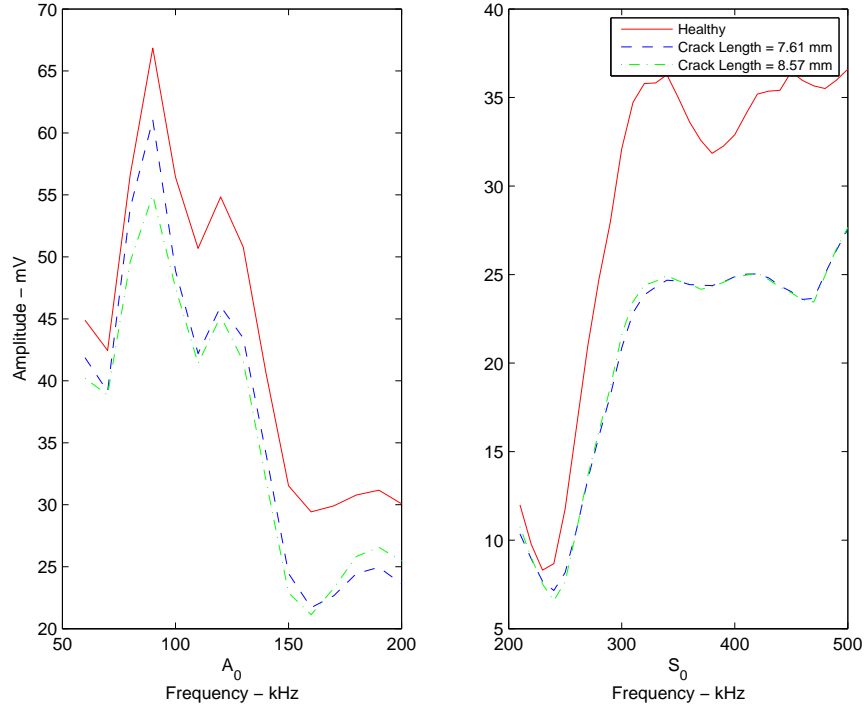
Figure 4.14:   Response amplitude exciting PZT 3, measuring
PZT 5B in Plate 4, with respect to excitation frequency.

most of the excitation signal to pass to the measuring PZT. Looking at Figure 4.15
the amount of excitation response being measured, in both the S_0 and A_0 windows,
decreases from the first crack length, to the second crack length, and again to the third
crack length. This is a good indication of being able to detected growing damage at
several frequencies in the A_0 and S_0 windows.

4.3.1.4   Plate 4, 4th Crack Increment.   After a total of 23,518 cycles, a
21.38 mm crack is present in the test plate. With a 21.38 mm crack, the propagation
paths of PZT pairs 1-5, 1-5B, 2-4, 2-4B, 2-6, 2-6, 3-5, and 3-5B are all interrupted by
the growing crack. We expect to see the response amplitude of PZTs 1-5 with a 21.38
mm crack , see Figure 4.16, show a marked decrease in either the S_0 of the A_0 window
when compared to the previous measurements.   While there is a decrease in the
response amplitude in the S_0 window between 200 and 360 kHz, the decrease is very
small. The decrease in response amplitude does not reflect the amount of excitation
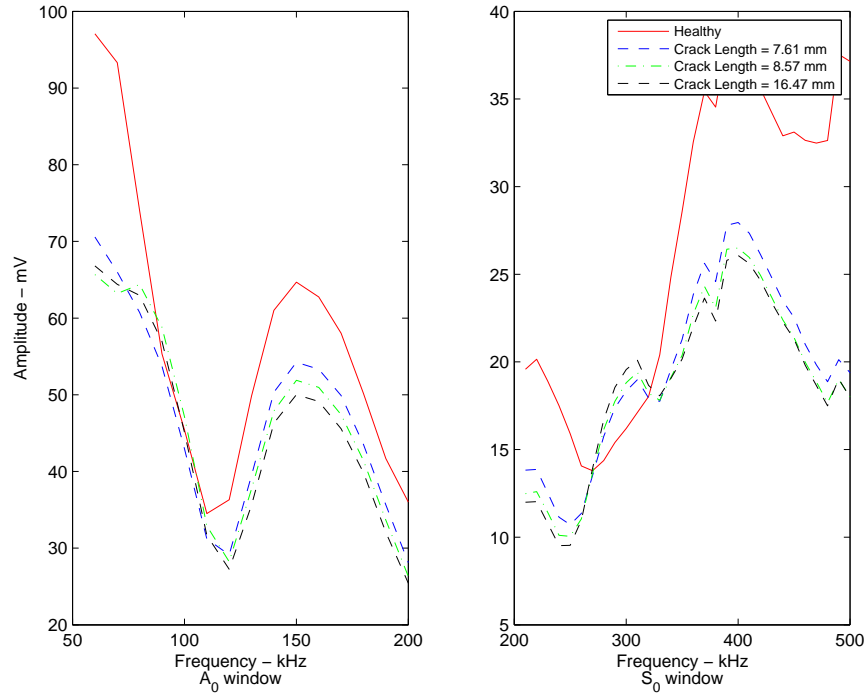
31

Figure 4.15:   Response exciting PZT 1, measuring PZT 6 in Plate 4, with respect to excitation frequency.
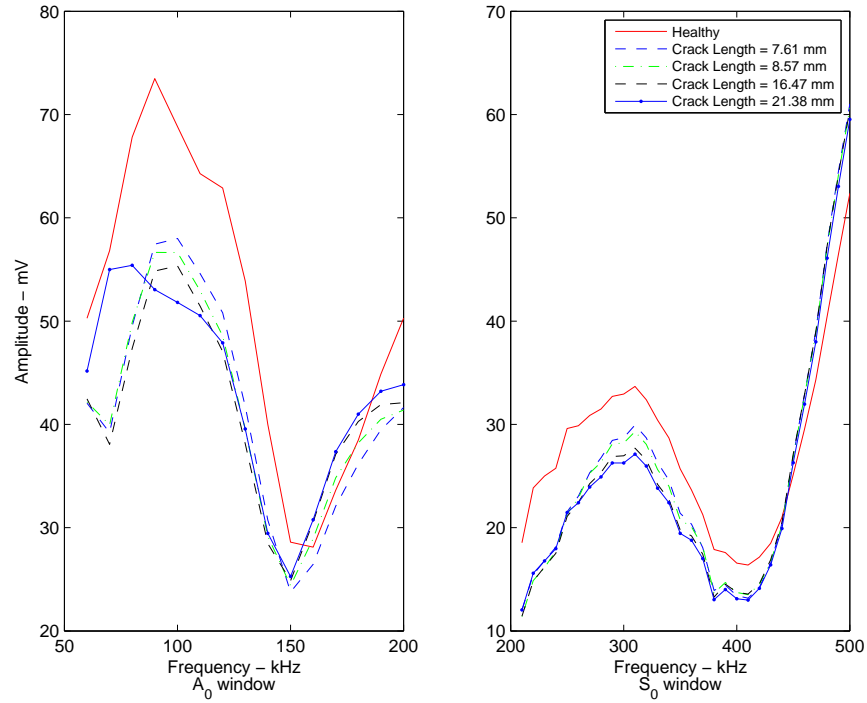

Figure 4.16:   Response exciting PZT 1, measuring PZT 5 in Plate 4, with respect to excitation frequency.

signal that we expected to be disrupted by the crack in the wave propagation path. Figure 4.17 shows a small increase in response amplitude between 200 and 360 kHz measured by PZT 6 when excited by PZT 2. The increase in response amplitude could indicate a number a issues dealing with damage in the plate and wave-crack interaction, but those scenarios are not accounted for in this analysis and thus not further explained.
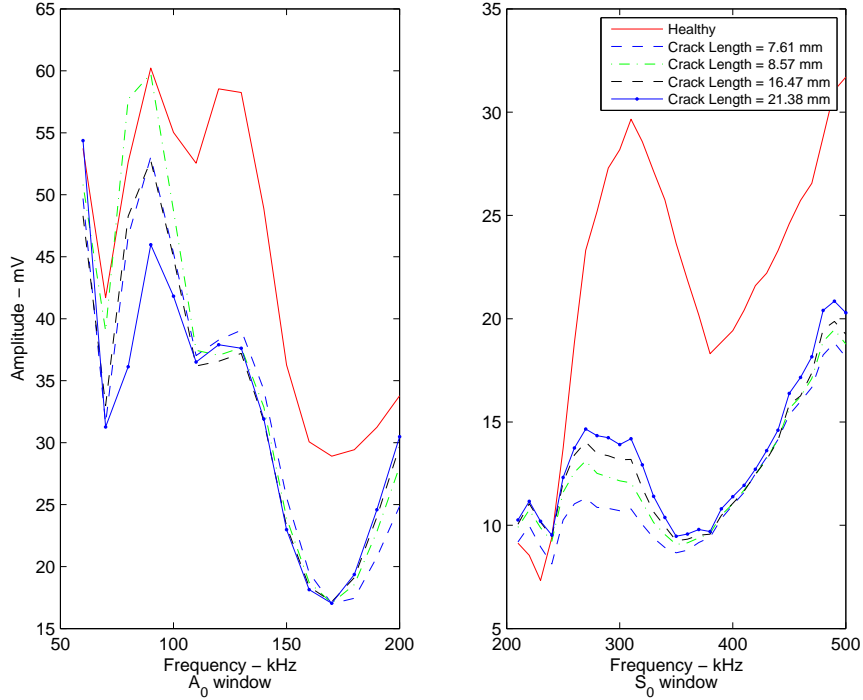
Figure 4.17:   Response exciting PZT 2, measuring PZT 6 in Plate 4, with respect to excitation frequency.

4.3.1.5   Plate 4, 5th Crack Increment.   PZT pairs 1-6 and 3-4 show a decrease in response amplitude after each crack increment. With a crack length of 26.21 mm, the response amplitude should continue the trend of decreasing after each crack increment. Figure 4.18 shows PZT pair 1-6 decreases in response amplitude in the A_0 and S_0 windows measured at 26.21 mm crack when compared to the measured response amplitude after a 21.38 mm crack. The same trend is seen with PZT pair 3-4, shown in Figure 4.19. The decrease in response amplitude measured by PZT

33

pairs 1-6 and 3-4 indicates the growing crack is preventing the excitation signal from propagating to the receiving PZT, correctly indicating signs of growing damage.
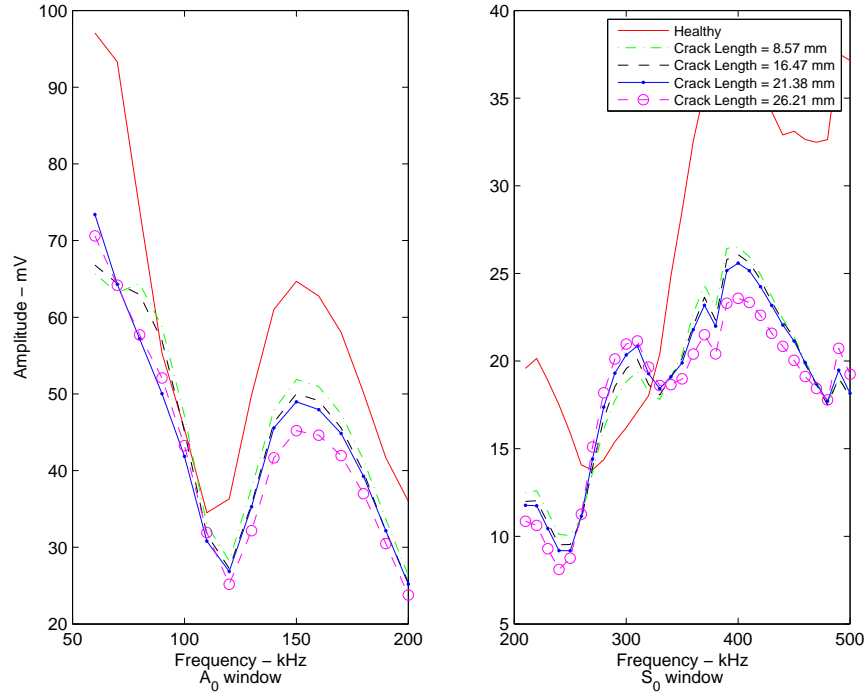
Figure 4.18:   Response exciting PZT 1, measuring PZT 6 in Plate 4, with respect to excitation frequency.

Similar to PZT pair 3-4, we expect PZT pair 3-5 to show a decrease in measured response amplitude in either the A_0 or S_0 window at a crack length of 26.21 mm when compared to the response amplitude measured at a crack length of 21.38 mm. Figure 4.20 shows a decrease in the peak response amplitudes measured from PZT pair 3-5 in the A_0 and S_0 windows. The decrease in response amplitude is small even at the peak values, and not a glaring indication of damage.

4.3.1.6   Plate 4, 6th Crack Increment.   The final crack length propagated in Plate 4 is 29.55 mm. We expected that the crack should be detectable by a decrease in response amplitude in PZT pairs 1-5, 1-5B, 2-4, 2-4B, 2-6, 2-6B, 3-5, and 3-5B because the crack intersects the wave propagation paths of all of these sensor paths. For example PZT pair 1-5 has a propagation path that was intersected when

34

Figure 4.19:   Response exciting PZT 3, measuring PZT 4 in Plate 4, with respect to excitation frequency.

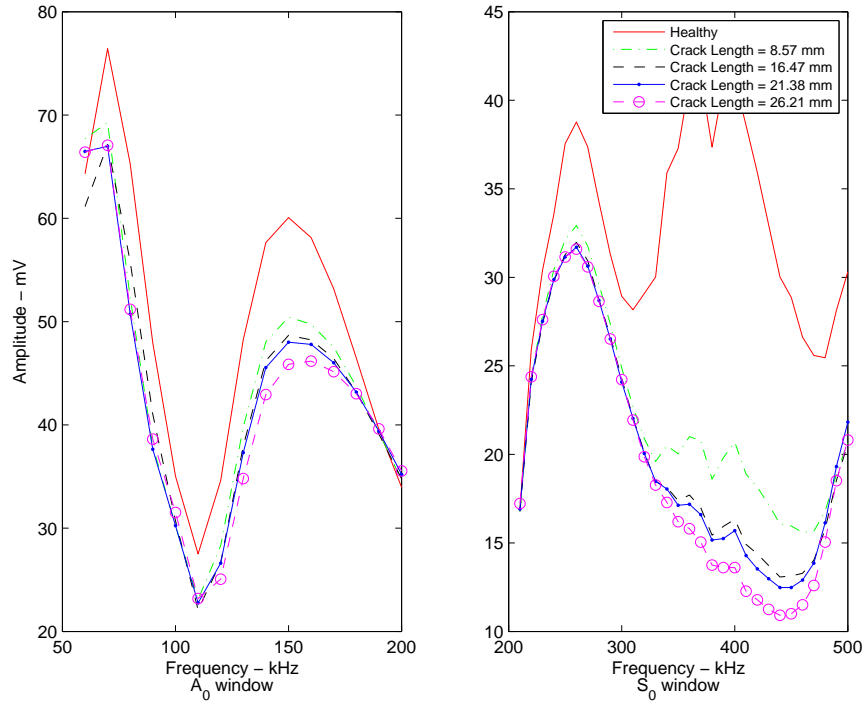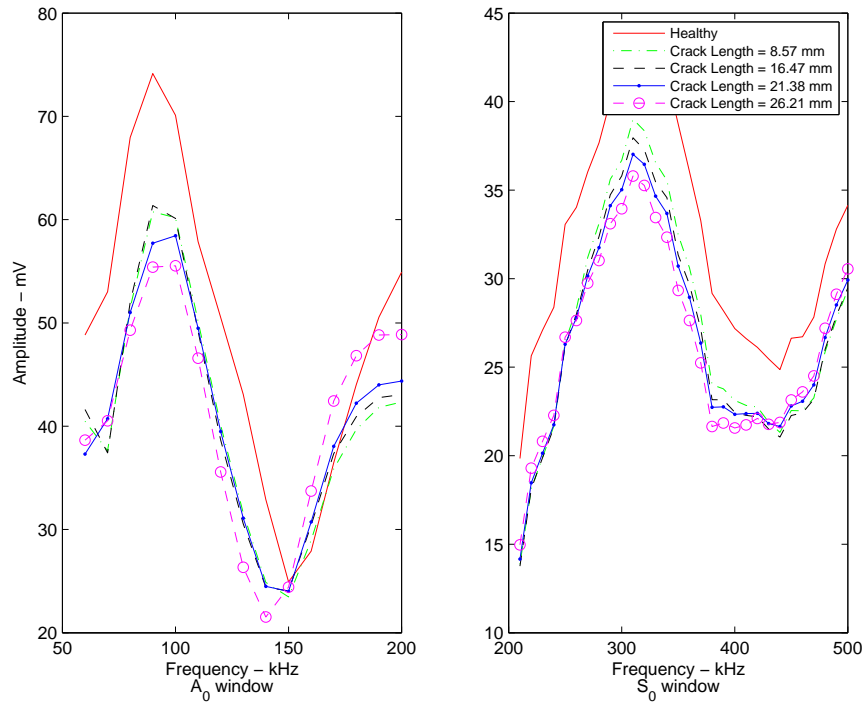Figure 4.20:   Response exciting PZT 3, measuring PZT 5 in Plate 4, with respect to excitation frequency.

the crack was propagated to a length of 20 mm, but before the crack reached 20 mm, the PZT pair 1-5 had an un-interrupted wave propagation path. Figure 4.21 shows the response amplitudes of PZT pair 1-5 for crack lengths of 8.57 mm, 16.47 mm, and 21.38 mm to be similar in amplitude in the S_0 window between 200 and 500 kHz. The response amplitude for PZT pair 1-5 noticeably decreases when the crack length reaches 29.55 mm, as seen in Figure 4.21. The same is true of PZT pair 3-5 (located on the opposite side of the rivet hole as seen in Figure 4.9), the response amplitudes are clustered together in the S_0 window at crack lengths of 8.57 mm, 16.47 mm, and 21.38 mm. The S_0 response amplitude decreases when the crack length reaches 29.55 mm in the window in Figure 4.22.

Figure 4.21: Frequency response exciting PZT 1, measuring PZT 5 in Plate 4, with respect to excitation frequency.

The PZT pairs 1-6, 1-6B, 3-4, and 3-4B show gradual decreases in response amplitude as the crack propagates. This trend continues as the crack grows, which can be seen in Figures 4.23 and 4.24. The PZT pair 3-4 indicates a less and less excitation signal being received by the measuring PZT as the crack propagates. This
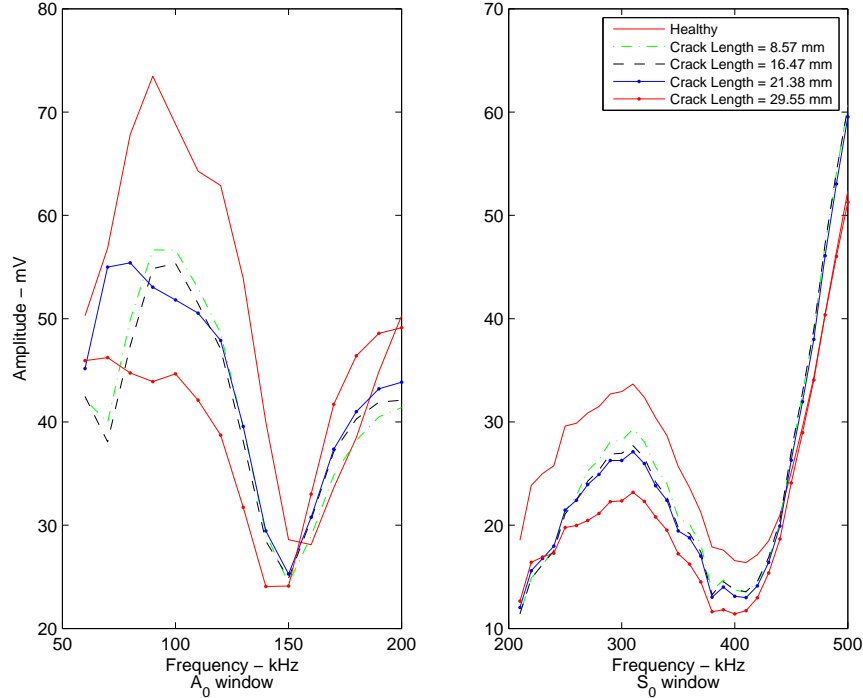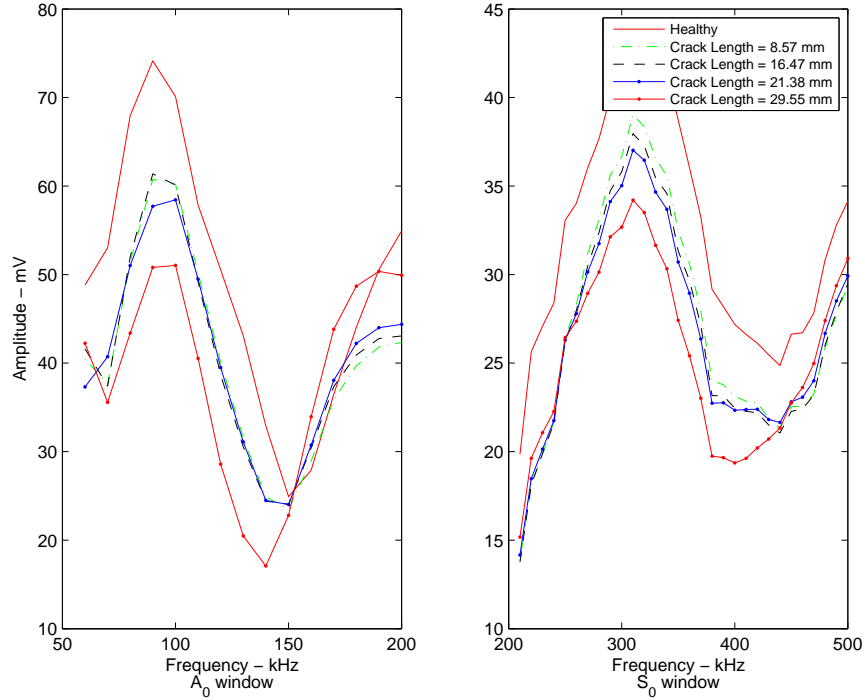
Figure 4.22:   Frequency response exciting PZT 3, measuring PZT 5 in Plate 4, with respect to excitation frequency.

is evident in the A_0 at 150 kHz and in the S_0 window between 320 and 450 kHz, Figure 4.23.

Test Plate 4 shows the potential for detecting damage with several combinations of PZT pairs, however the indications of damage are not comparable to the results seen when a cut was used to simulate damage by Crider [7]. Test Plate 5 increases the static loading to increase the indications of damage [11].

4.3.2 Test Plate 5.   The goal of this experiment is to detect a closed crack, but as seen in test plate 4, a closed crack can be difficult to detect. Because we are interested in increasing the probability of detecting the presence of a crack, we expand the crack size opening by increasing the static load [11]. Therefore, data is collected under four static loads: 100, 4,000, 6,000, and 8,000 lbs at each crack length interval. We considered the crack closed with the 100 lb static load on the plate, and open under the 4,000, 6,000, and 8,000 lb static loads. The applied loads resulted in

37

Figure 4.23: Response exciting PZT 3, measuring PZT 4 in Plate 4, with respect to excitation frequency.
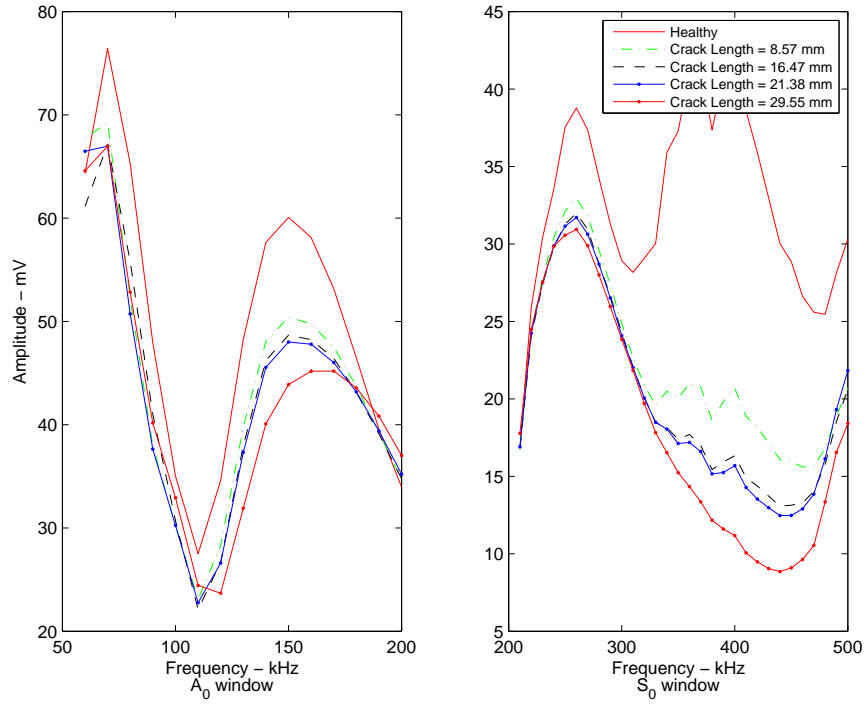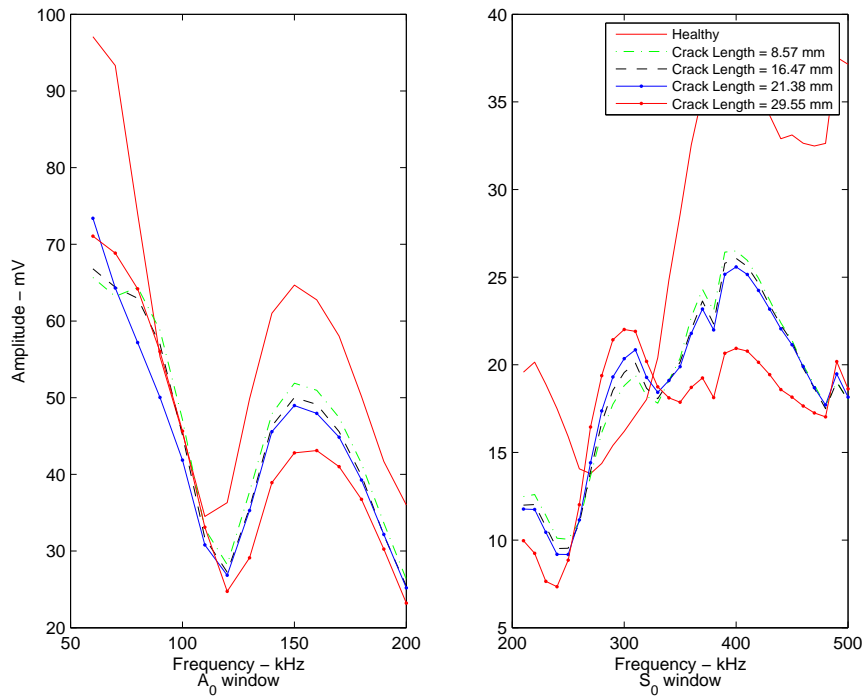

Figure 4.24: Response exciting PZT 1, measuring PZT 6 in Plate 4, with respect to excitation frequency.

a maximum stress of 79% of the yield stress for 6061-T6 aluminum [8] in the bulk of the plate, but exceeded yield at the simulated rivet hole causing microscopic damage to the plate. The loads shown in Table 4.2 are not necessarily representative of actual loading an aircraft bulkhead would experience in flight or on the ground, but were selected to grow a crack in a timely manner.

Table 4.2: Loading schedule and crack length for test plate 5.

Cyclic Loading		
Load(kips)	Cycles	Crack Length(mm)
13 - 1.3	6,000	1.67*
13 - 1.3	6,000	3.77
13 - 1.3	2,000	5.21*
11 - 1.1	4,000	13.96*
9 - 0.9	3,000	18.34*
7 - 0.7	4,000	18.64
7 - 0.7	4,000	18.94
8 - 0.8	2,000	21.85
8 - 0.8	1,000	27.85*
6 - 0.6	2,000	28.47
7 - 0.7	2,000	35.90*

* data collected

Before propagating fatigue cracks in the test plate 5, data is collected at 100, 4,000, 6,000, and 8,000 lbs to form a baseline of healthy responses. The healthy responses were evaluated to establish behavior of the PZTs under the four different static loads. Figure 4.25 shows the amplitude measured from PZT pair 3-4 at 80 kHz decreases as the static load is increased. Figure 4.26 shows the response amplitude of the same pair through out the entire excitation frequency range.

Since the amount of response amplitude is effected by the amount of static load, only measurements taken under the same loading conditions can be compared to each other. For a real SHM system this means that if the system must be operated in flight, the same flight conditions must be repeated each time data is to be collected. Repeating the same flight conditions is a challenging proposition, and could limit the application of this technology.
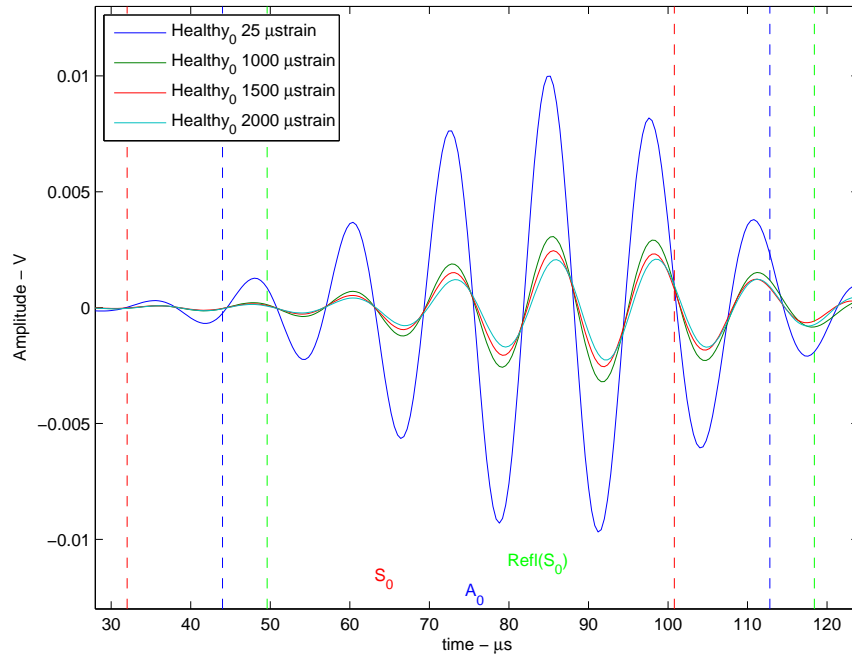
Figure 4.25: Decrease in response output of PZT 4 when excited from PZT 3 at 80 kHz, as static load increases in Plate 5.
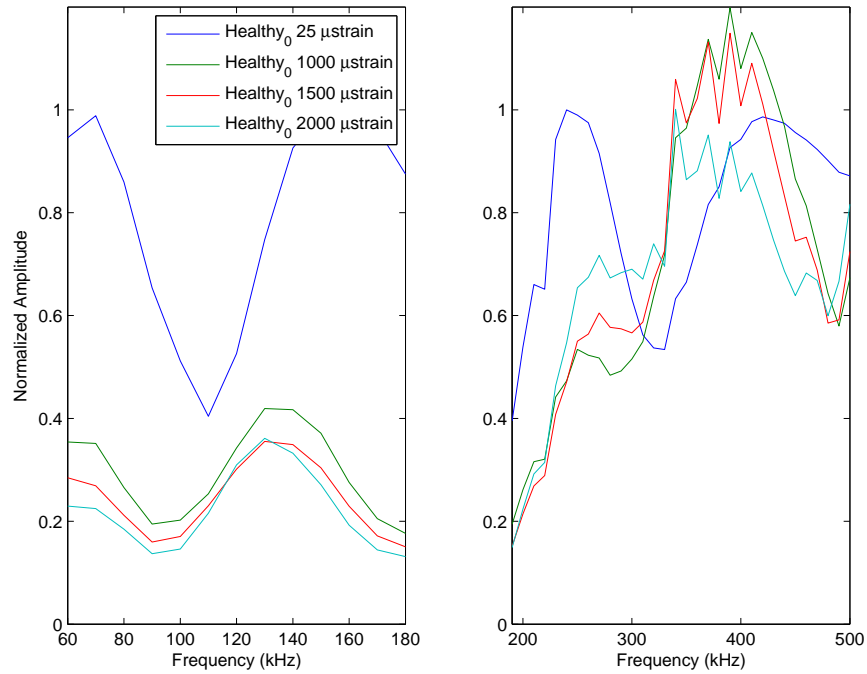

Figure 4.26: Decrease in response output through out the excitation frequency range as static load increases in Plate 5.

After 6,000 cycles of fatigue loading to forces of 13 to 1.3 kips (where the PZT and plate experience a peak strain of 3,300 μstrain), an additional set of baseline healthy data is collected at 100, 4,000, 6,000, and 8,000 lbs and compared to the initial healthy responses. No visual damage was detected at 6,000 cycles, but the amplitude of the responses of all six of the PZTs decreased when excited by all three of the actuating PZTs, as seen in Figure 4.27. This decrease in response amplitude is a potential degradation of the sensor due to over straining the PZT material [11]. Since we continue use these sensors and the 13 kip (3,300 μstrain) load is the max load experienced by the PZT, it makes sense to consider this state the healthy baseline.
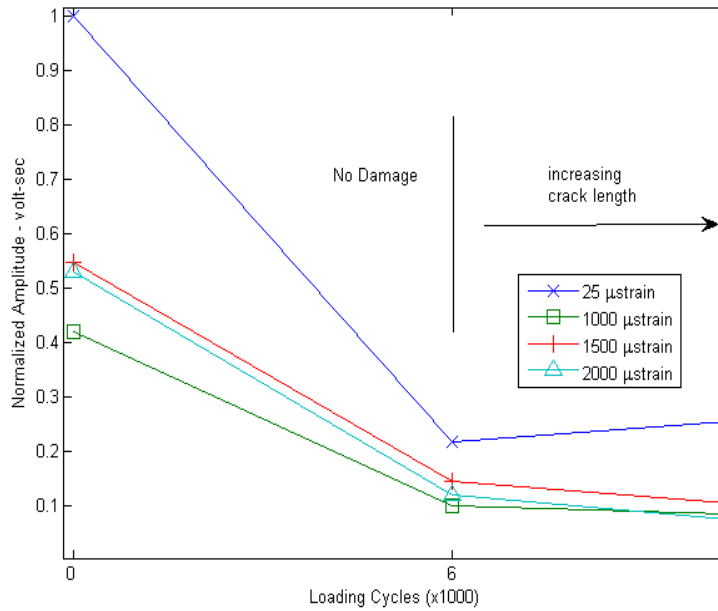
Figure 4.27: Decrease in response amplitude of PZT 4 when excited from PZT 3 at 80 kHz, as static load increases, after 6,000 cycles at 3,300μstrain on Plate 5.

4.3.2.1 Plate 5, 1st Crack Increment. The response amplitude decreases after the first 6,000 cycles, as shown in Figure 4.27, but it continues to decrease as the plate experiences 8,000 more fatigue loading cycles at 13 to 1.3 kips. Figure 4.28 shows the response amplitudes decrease at all four static loads as fatigue loading

continues. The decrease in response amplitude due to fatigue loading is consistent
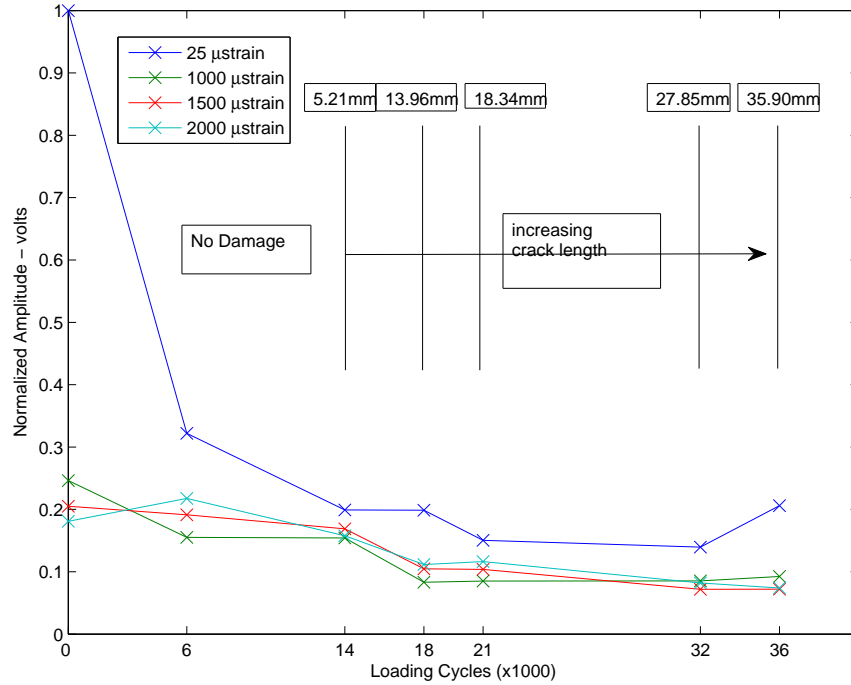
Figure 4.28: Decrease in response amplitude of PZT pair 2-6 excited at 130 kHz as static load increases and with fatigue loading on Plate 5.

through the first 14,000 cycles for all the PZT pairs. Therefore, the first crack length is undetectable closed or open, as it is masked by the decrease in response amplitude cause by the fatigue loading.

4.3.2.2 Plate 5, 2nd Crack Increment. The response amplitude decrease due to fatigue effect, as seen at the previous crack length increment (Figure 4.28) should be negligible after 18,000 cycles of fatigue loading. Therefore, the response of PZT pair 1-5 should not decrease in amplitude when measured at a crack length 13.96 mm and compared to the measurement taken at a crack length of 5.21 mm. Figure 4.29 shows a decrease in response amplitude measured at a crack length of 13.96 mm when compared to the measured response taken at a crack length of 5.21 mm. The same trend is shown by PZT pair 2-6, in Figure 4.30.

42

Figure 4.29: Response exciting PZT 1, measuring PZT 5 with a 100 lb static load on Plate 5, with respect to excitation frequency.

Figure 4.30: Response exciting PZT 2, measuring PZT 6 with a 100 lb static load on Plate 5, with respect to excitation frequency.

This must mean either the fatigue loading is still impacting the measurements, or the presence of a crack in the plate is decreasing the amount of excitation signal being transmitted to the receiving PZT, even though the crack does not intersect the wave propagation path of the PZT pair. Figures 4.29 and 4.30 are results taken at a 100 lb static load. We would expect the decrease in amplitude to continue as an increase static load is applied. Figure 4.31 shows the response of PZT pair 1-5 measured under a 4,000 lb static load. The responses are approximately equal in the A_0 window, but the response in the S_0 window with a 13.96 mm crack decreases from the response with a 5.21 mm crack. The same trend of response amplitudes decreasing in the S_0 window is seen in Figures 4.32 and 4.33 as the static load is increased to 6,000 and 8,000 lb respectively.

Figure 4.31: Response exciting PZT 1, measuring PZT 5 with a 4,000 lb static load on Plate 5, with respect to excitation frequency.

The results of measuring PZT pair 1-5 shows increasing the static load tends to increase the difference in measurements. However, in the case of PZT pair 1-5 with
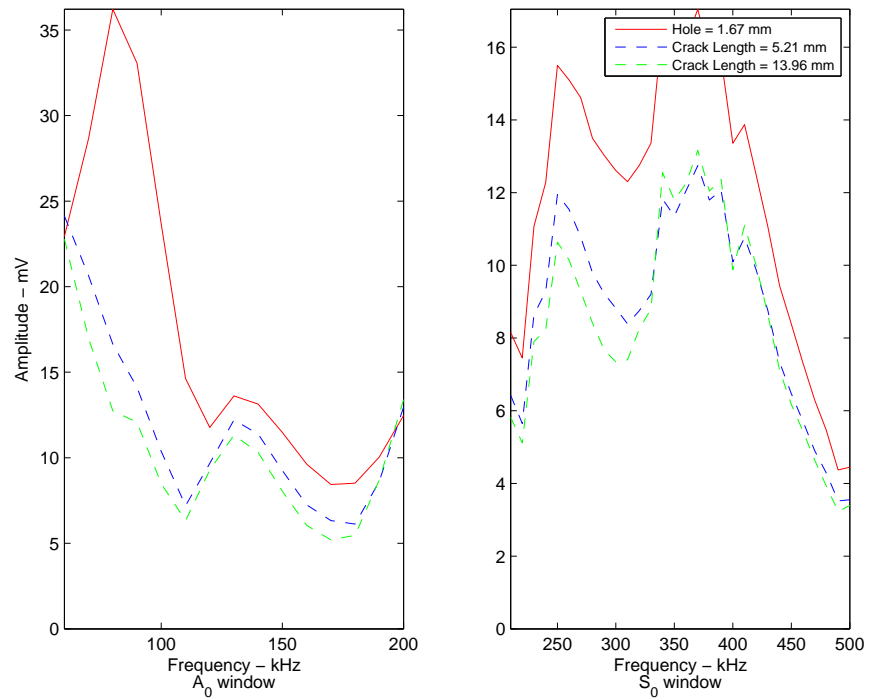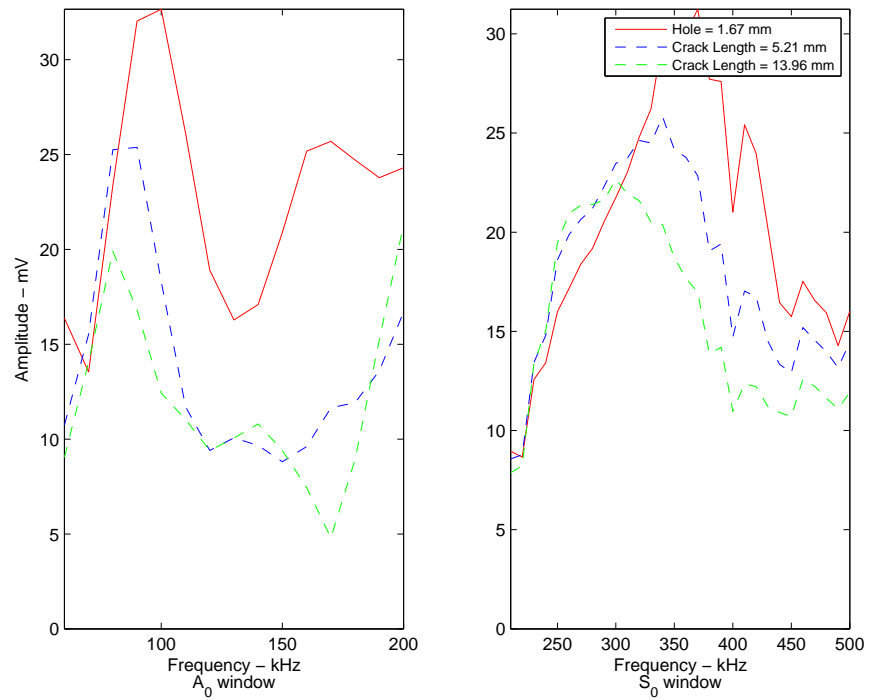
Figure 4.32: Response exciting PZT 1, measuring PZT 5 with a 6,000 lb static load on Plate 5, with respect to excitation frequency.

Figure 4.33: Response exciting PZT 1, measuring PZT 5 with a 8,000 lb static load on Plate 5, with respect to excitation frequency.

a crack length of 13.96 mm present in the test plate, there should not be a decrease in response amplitude. To be an indicator of damage a response amplitude will need to be a marked decrease from the response amplitudes measured after crack lengths of 5.21 mm and 13.96 mm.

4.3.2.3 Plate 5, 3rd Crack Increment.   Test Plate 4 showed a decrease in response amplitude in the cross-plate PZT pairs 1-6, 1-6B, 3-4, and 3-4B at the third crack length, therefore we expect Test Plate 5 to also display a amplitude decrease when exciting PZT 1 and measure PZT 6. Figure 4.34 shows a gradual decrease in the peak amplitude in the S_0 window. The same PZT pair shows a larger separation in the response amplitudes in Figure 4.35 between the 5.21 mm crack length and the 13.96 mm crack length with a 4,000 lb static load applied to the plate. The separation in the S_0 window between the responses at 5.21 mm, 13.96 mm, and 18.34 mm gets larger as more static load is applied, shown in Figures 4.36 and 4.35.

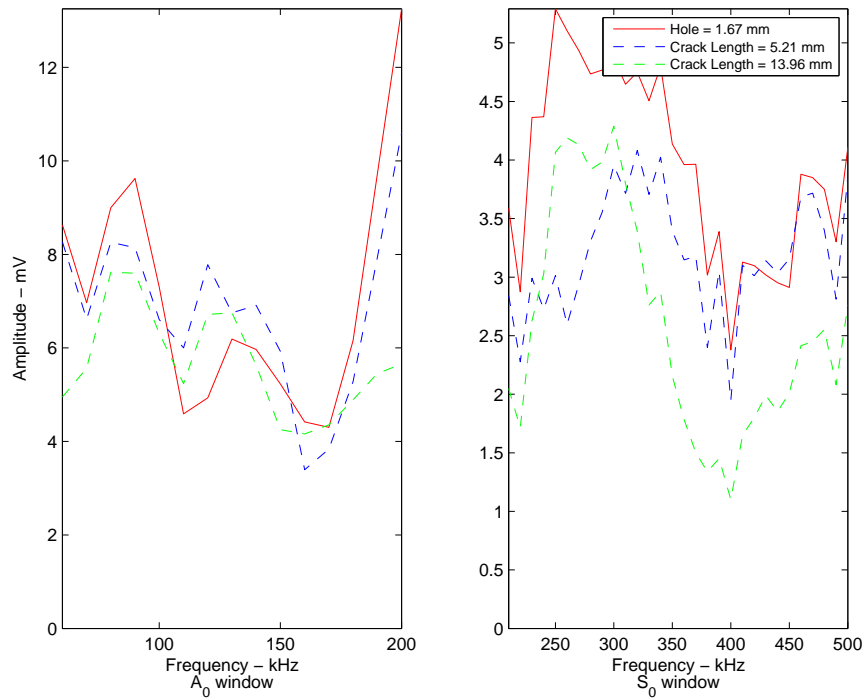Figure 4.34:   Response exciting PZT 1, measuring PZT 6 with a 100 lb static load on Plate 5, with respect to excitation frequency.

Figure 4.35: Response exciting PZT 1, measuring PZT 6 with a 4,000 lb static load on Plate 5, with respect to excitation frequency.
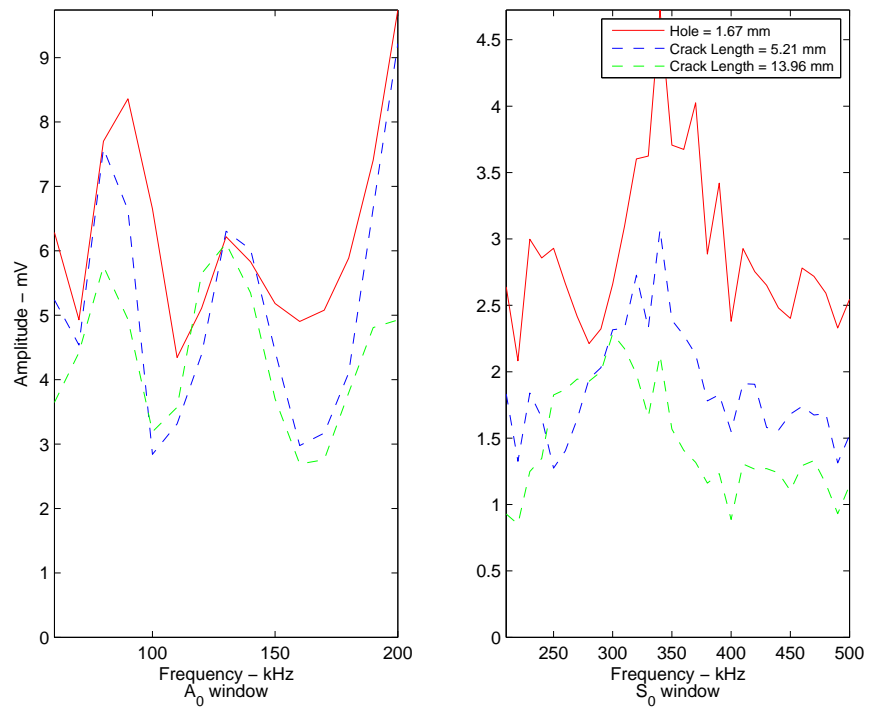
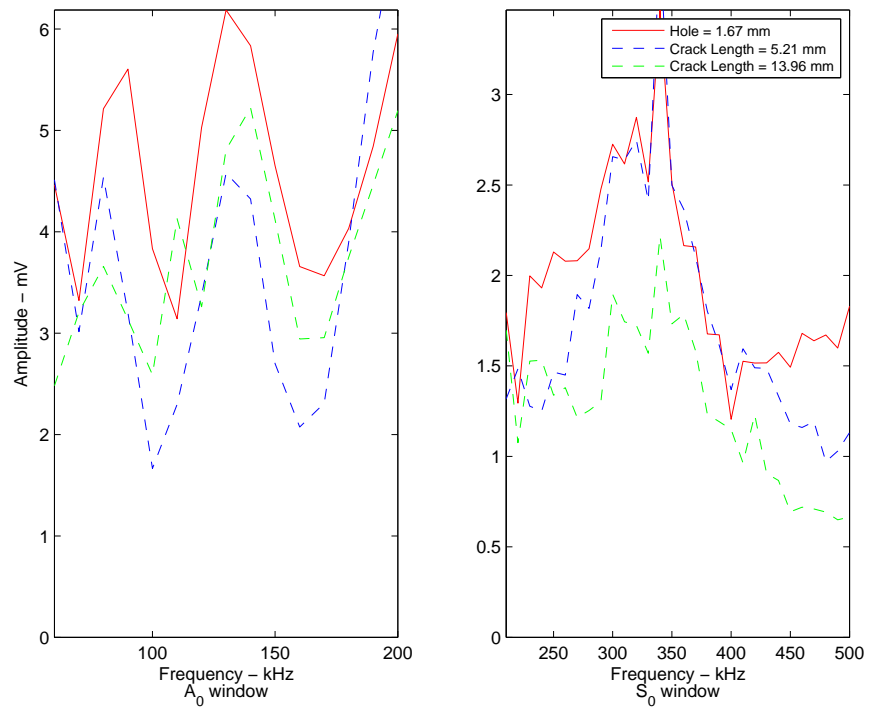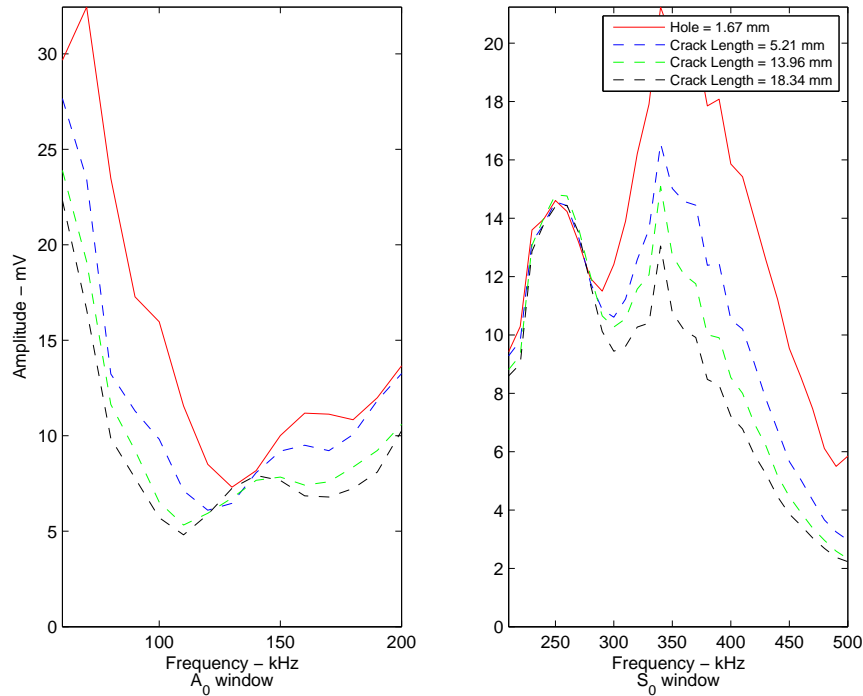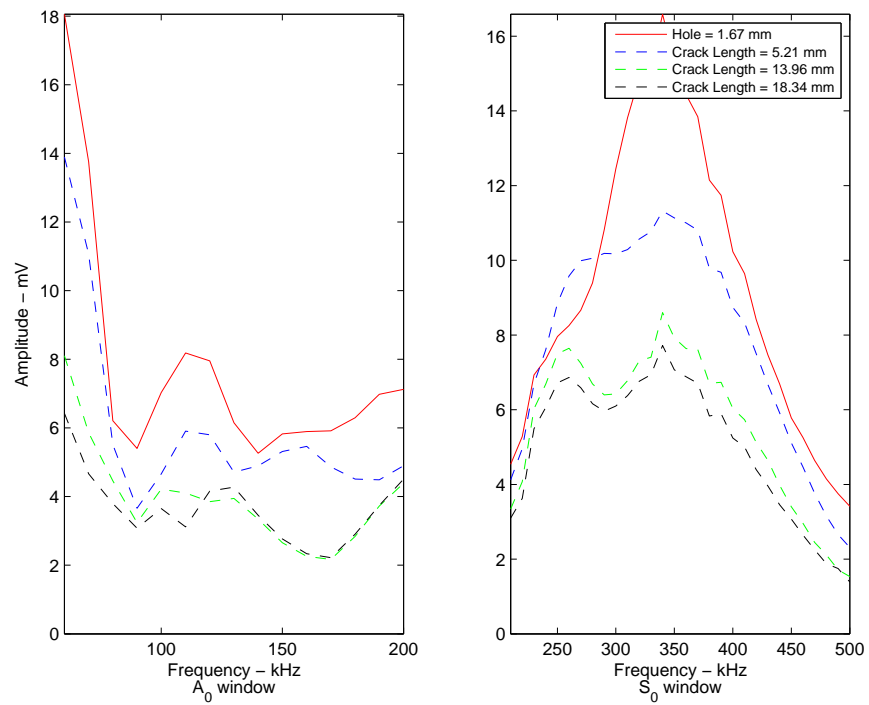Figure 4.36: Response exciting PZT 1, measuring PZT 6 with a 6,000 lb static load on Plate 5, with respect to excitation frequency.

Figure 4.37:   Response exciting PZT 1, measuring PZT 6 with a 8,000 lb static load on Plate 5, with respect to excitation frequency.

The decrease in response amplitudes at each longer crack length is a good indication of a growing crack. The addition of a larger static load highlights the decrease in response amplitude, thus increasing the potential of damage detection.

4.3.2.4 Plate 5, 4th Crack Increment.   With a crack length of 27.85 mm in the center of the plate, PZT pairs 1-5, 1-5B, 2-4, 2-4B, 2-6, 2-6B, 3-5, and 3-5B should show a decrease in amplitude when compared the previous crack lengths. Figure 4.38 shows a decrease in the response amplitude in the S_0 window between 250 and 500 kHz, measured at a crack length of 27.85 mm, but the decrease is a similar to the decreases seen between the previous crack length increments.

Figure 4.38:   Response exciting PZT 2, measuring PZT 6 with a 100 lb static load on Plate 5, with respect to excitation frequency.

Increasing the static load should decrease the response amplitude of PZT 2-6, hopefully distinguishing the response amplitude measured at 27.85 mm from the responses measured at previous crack lengths. Figures 4.39, 4.40, and 4.41 show the

measured response from PZT pair 2-6 under a 4,000, 6,000, and 8,000 lb static loads, respectively. The increased static load decreases the response amplitude measured

Figure 4.39: Response exciting PZT 2, measuring PZT 6 with a 4,000 lb static load on Plate 5, with respect to excitation frequency.

at a 27.85 mm crack in the plate but, like Figure 4.38 the decreases are similar to the response amplitude decreases at the previous crack lengths.

4.3.2.5 Plate 5, 5th Crack Increment. The final crack increment is 35.90 mm across the center of the test plate. The crack intersects the wave propagation path of PZTs 2-6. Even at a 100 lb static load, the response amplitude decreases noticeable at 450 kHz in the S_0 window, Figure 4.42. When the crack is opened with an 8,000 lb load, Figure 4.43, the response amplitude of PZT pair 2-6 decreases through out the S_0 window. The potential of detecting damage between 200 and 500 kHz is high in the path between PZTs 2-6.

Figure 4.40: Response exciting PZT 2, measuring PZT 6 with a 6,000 lb static load on Plate 5, with respect to excitation frequency.

Figure 4.41: Response exciting PZT 2, measuring PZT 6 with a 8,000 lb static load on Plate 5, with respect to excitation frequency.
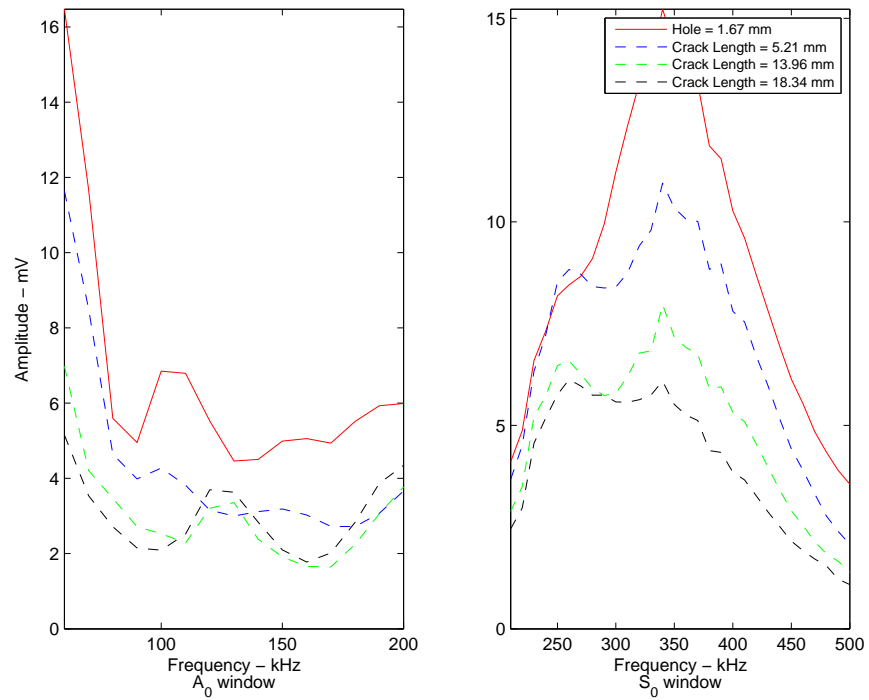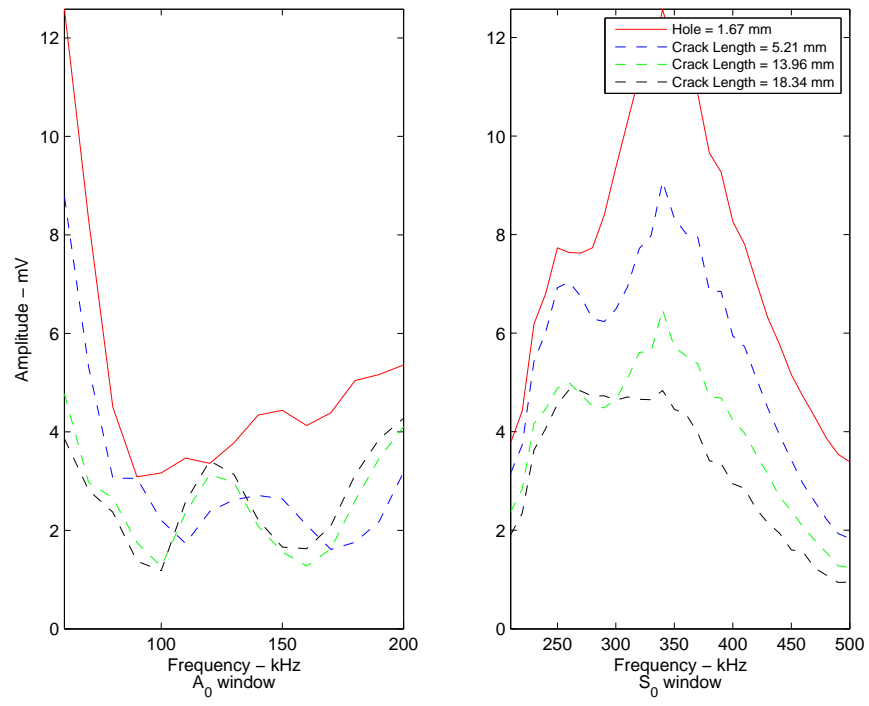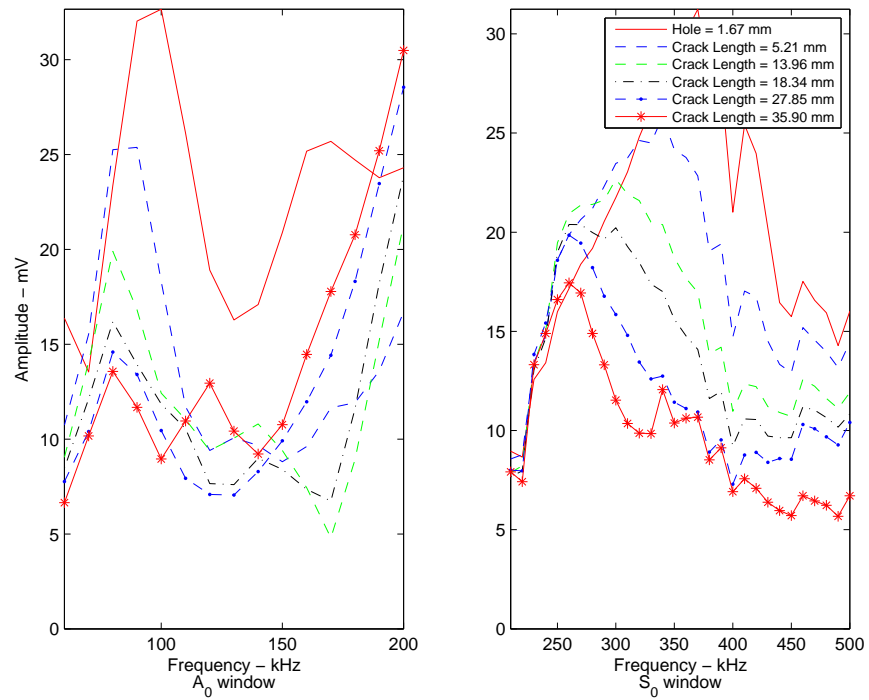
Figure 4.42: Response exciting PZT 2, measuring PZT 6 with a 100 lb static load on Plate 5, with respect to excitation frequency.
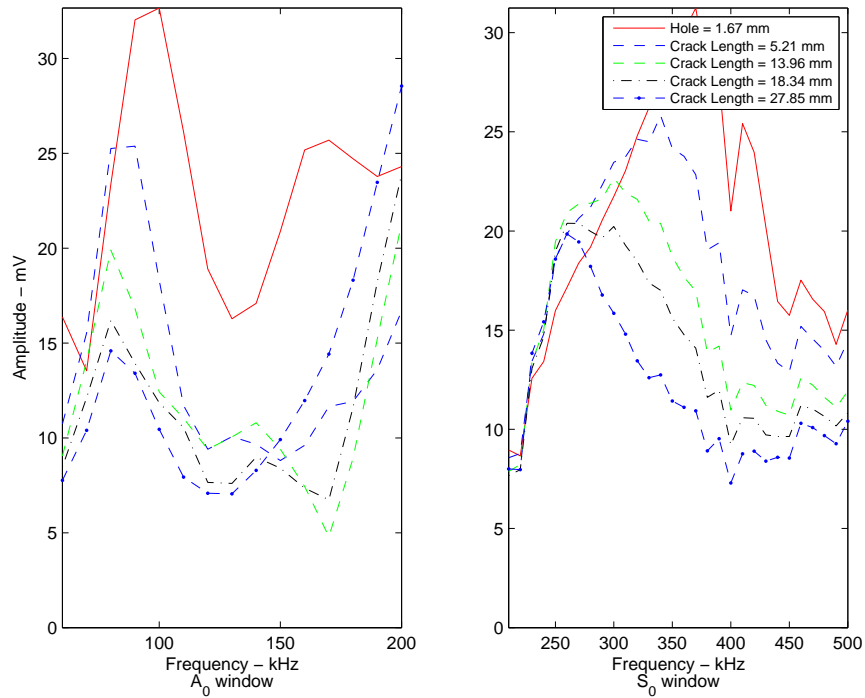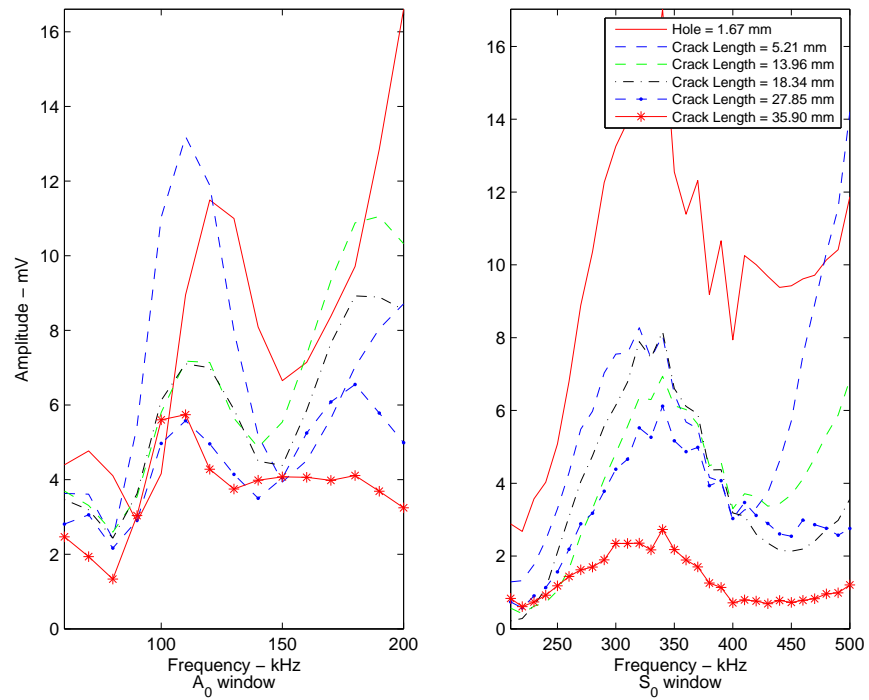
Figure 4.43:   Response exciting PZT 2, measuring PZT 6 with
a 8,000 lb static load on Plate 5, with respect to excitation
frequency.

Examining the cross plate PZT pair 1-6 shows the peak response amplitude in the S_0 window gradually decrease, when measured with a closed crack, as the crack propagates across the plate (Figure 4.44). The peak response amplitude in the S_0 window decreases drastically as the crack propagates across the plate, when measured under an 8,000 lb static load, as seen in Figure 4.45.
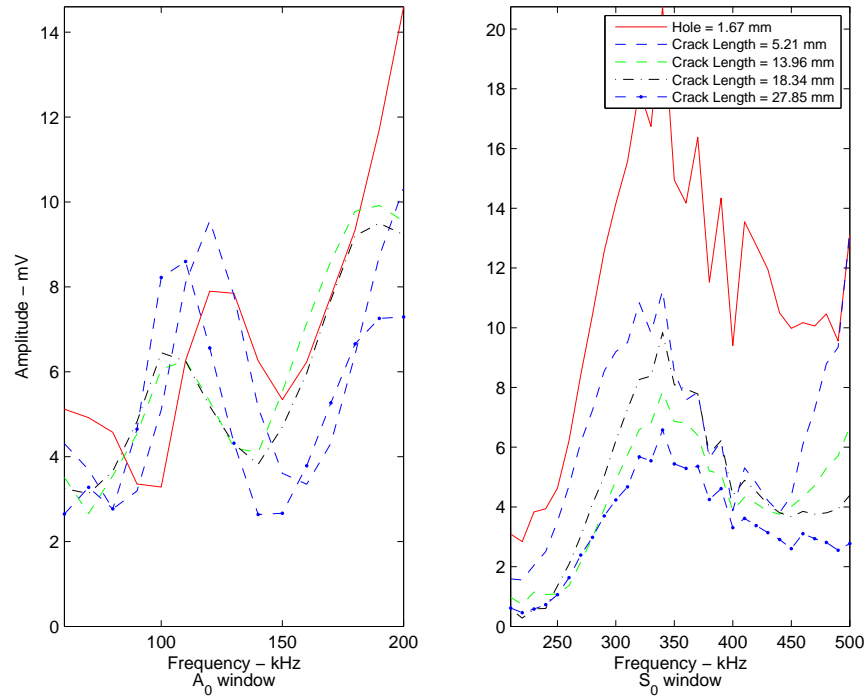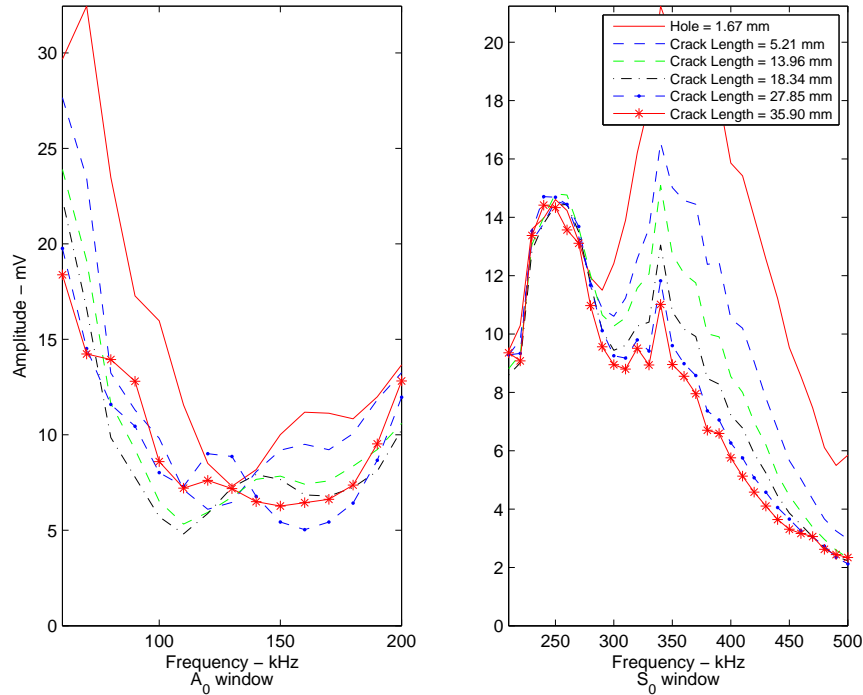

Figure 4.44:   Response exciting PZT 1, measuring PZT 6 with a 100 lb static load on Plate 5, with respect to excitation frequency.

Plate 5 accomplished the goals of this thesis by highlighting indications of damage in the plate. With an increased static load opening the crack in the plate, the amount of response amplitude decreased more than when the crack was considered closed. Plate 5 also brought to light the challenges of using PZTs in a fatigue loading environment. The challenges and successes of Plate 5 provide a roadmap for future research in the are of damage detection using PZTs to generate Lamb waves in a thin sheet of aluminum.
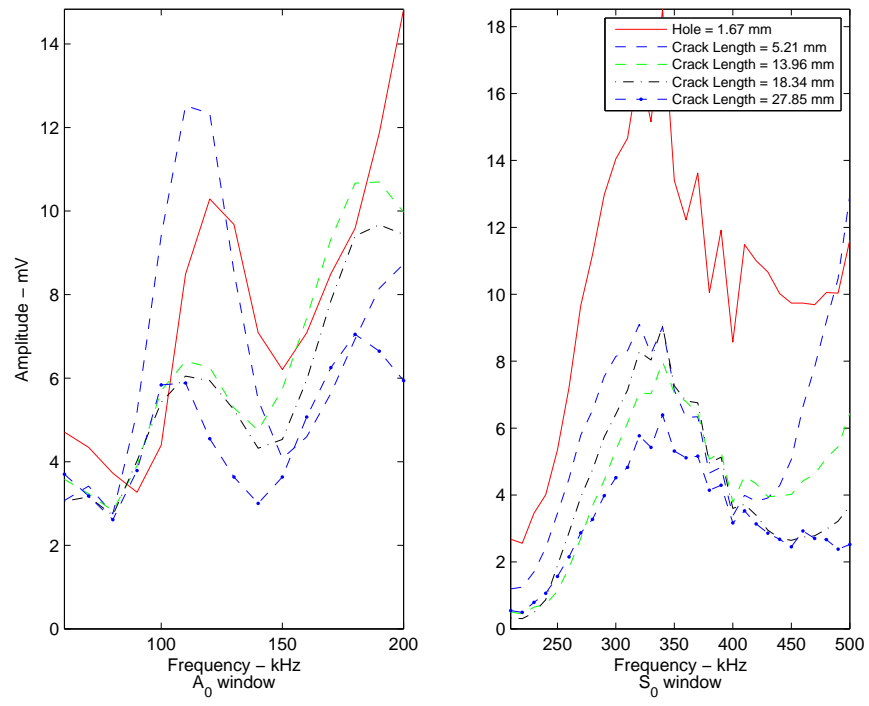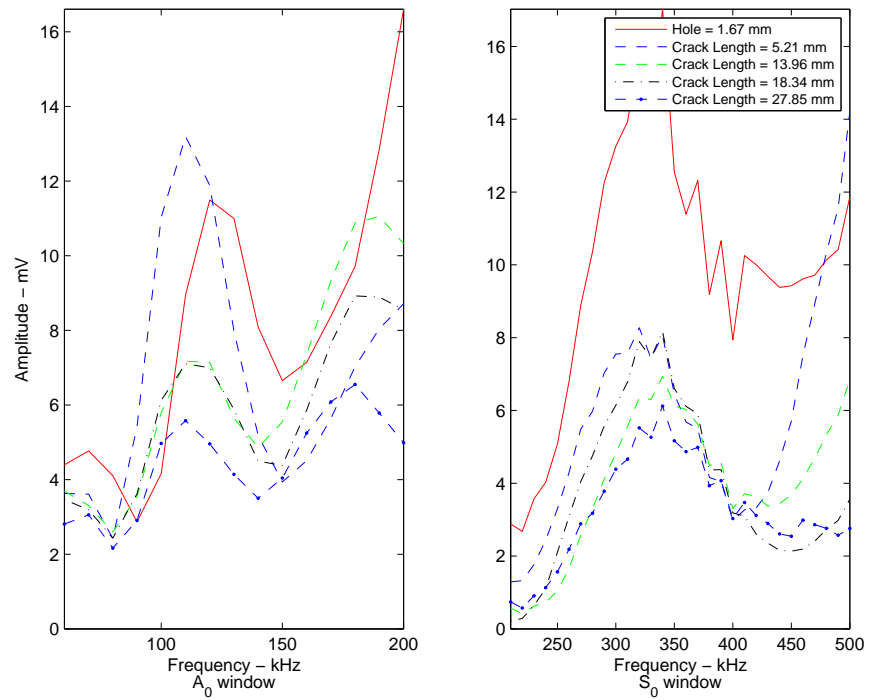
Figure 4.45: Response exciting PZT 1, measuring PZT 6 with a 8,000 lb static load on Plate 5, with respect to excitation frequency.
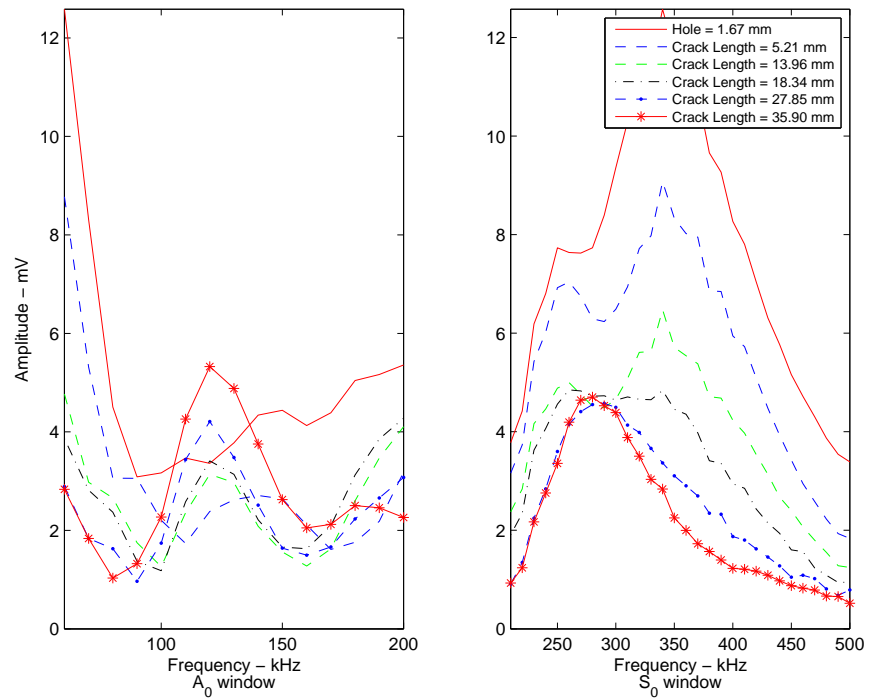
V. Conclusions

The goal of this thesis is to determine if PZT sensors can be used to detect a propagated fatigue crack in restricted geometry representative of an actual F-15 bulkhead. The study was carried out with a series of three tests, as discussed in Chapters III and IV, involving Lamb wave characterization on a large flat plate and the use of Lamb waves to detect a propagated fatigue crack. We will now discuss the outcome of this thesis research including lessons learned form the LFP and the damage detection results from the bulkhead-webbing experiment.

5.1 LFP Discussion

The first experiment in this thesis research involved using four PZT discs attached to a 24" x 48" x 1/8" sheet of 6061-T6 aluminum (refereed to as the LFP). The purpose of the LFP experiment is to develop our test method, gage our ability to predict TOA windows, and determine the usefulness of mode isolation. Four test phases utilized four PZT discs to produce and sense Lamb waves in the aluminum sheet using a "pitch-catch" approach. Phase one of the experiment excited Lamb waves at one PZT and received the signal at one PZT located on the same side of the plate as the exciting PZT. Phase two of the experiment excites two PZTs, front-to-back with respect to each other, simultaneously in phase to cancel out the A_0 mode of the Lamb wave signal. Phase three simultaneously excites two front-to-back PZTs 180 degrees out of phase with each other to cancel out the S_0 mode of the Lamb wave signal. Finally, phase four of the experiment measures the response at two front-to-back PZTs when Lamb waves are excited from only one PZT.

The LFP experiment produced useful results in that we determined we were able to predict the arrival windows for the S_0 and A_0 waveforms, as seen in Figure 4.1. Phase four of the LFP experiment confirmed our window prediction by identifying the wave modes in our prediction windows. Efforts were made to use dual excitation of front-to-back PZTs for mode isolation, shown in Figures 4.2 - 4.7. Some successes were seen with this method to cancel out the S_0 or A_0 mode, but mostly the method

60

was inconsistent and limited. No further study was done with dual excitation for mode isolation. Figure 4.8 shows the results of using two sensors to simultaneously measure the excitation signal. Although each PZT disc has a different gain, or individual amplitude, the signals are clearly seen to be in phase with each other during the S_0 mode and 180 degrees out of phase with each other during the A_0 mode. Identifying the waveforms is the most useful addition to this research by mode isolation. Using two PZTs cancel out an excited wave form by simultaneous excitation is not an effect method of mode isolation and no further research conducted with that method. However, the potential of using front-to-back PZTs to receive Lamb waves and then post-process the response for mode isolation should potential for increasing damage detection capabilities. Therefore, the bulkhead-webbing experiment test specimen were instrumented with PZTs to receive front and back responses.

5.2   F-15 Bulkhead Damage Detection

Two test plates with restrictive geometry similar to that of an F-15 bulkhead where used to propagate fatigue cracks. Figure 3.5 (a) and (b) shows the PZTs configured on each test plate. The configuration used is similar to the configuration that could be used to monitor an F-15 bulkhead. The plates where cyclically loaded, to a maximum strain of 3,300 μstrain, to propagate a crack in increments. At each increment, measurements where taken with a "pitch-catch" method to measure the response amplitudes as defined by the Equations (4.1) and (4.2).

The results we chose to analyze are from the PZTs pairs with oblique wave propagation paths. By choosing the pairs with oblique wave propagation paths we were able to minimize the interference of reflected waves. Of the pairs we chose, two groups exists: those paths that include the rivet hole and the propagated crack at all increments, and those paths that do not include the rivet and only encounter the crack after the crack propagates 10 mm on either side (20 mm total length).

The wave propagation paths that include the rivet hole and all crack lengths show the potential to successfully monitor crack growth. Since all measurements after

the healthy baseline (which can be discarded due to overstraining) include the crack, indication of a growing crack can be observed by a response amplitude amplitude decrease after each crack length increment at some frequencies in our excitation frequency range. With the addition of a large static load, to increase the opening of the crack, the response amplitude decrease is highlighted. Comparing Figure 4.23 (measured with a closed crack) to Figure 4.45 (measured with an open crack), the amount of response amplitude change between crack length increments is larger when the crack is open. The challenge to detecting an open crack is applying a consistent and repeatable load, since data samples must be compared under the same loading conditions. Therefore, in an F-15 a healthy baseline of data must be collected with the aircraft in flight. The SHM system must then periodically collect data at the same flight condition to compare to the healthy baseline.

While damage can be easier to detect when the part is under load, it is not impossible for damage to be detected without a load being applied to the part. The challenge to detecting damage without a load being applied, is to correctly identify a small amount of response amplitude decrease as damage. Looking at Figure 4.42 where the crack is considered to be closed, there is a 35% decrease in peak response amplitude between the fourth and the fifth crack length increments (when a crack is present and damage should be detected) when exciting between 400 and 500 kHz. In the same excitation frequency range the average decrease in peak response amplitude after each crack length increment is only 12%, therefore a 35% response amplitude decrease could be a good indication of damage. Comparing the response decreases at 100 lb (Figure 4.42) to the response decreases seen with an 8,000 lb static load opening the crack (Figure 4.43), the response decreases by 55% between the fourth and fifth crack length increments when exciting between 300 and 400 kHz. There is little response amplitude decrease in the same excitation frequency range between the other crack length increments, therefore the 55% decrease is a good indication of damage. Potentially, the 55% decrease would be easier to correctly identify as damage, but the 35% response decrease is also possible to detect and interrupt as

damage. It is important to be able to detect a closed crack because it is much easier to take repeated measurements at the same loading condition when the aircraft on the ground in a static environment.

The ability to detect damage as it occurs is a main goal of SHM. This thesis research explored the possibility of using PZT transducers to detect damage at various increments. We showed that detecting damage is possible with a closed crack, but the odds of detection are increased by increasing the static load to open the crack. However, collecting data on an F-15 in flight with the same load condition is not very practical. On the other hand, it is easy and more practical to repeatedly collect data on the ground in an unloaded condition. For a successful SHM system to be fielded on a F-15, the system must be able to be operated from the ground, and reliably interpreted by a field-level NDI technician. The ability to detect damage as it occurs may be possible with the use of PZT in a "pitch-catch" method, but more research and refinement are necessary to increase the reliability of damage detection.

5.3 Future Research

To create a viable and robust SHM system for the F-15 bulkhead, more research shoud be completed. Future research that should be accomplished to advance the use of PZT sensors to detect damage in a SHM role should include research to characterize PZT behavior in a high and low strain fatigue environments. Understanding the ability of PZTs to produce and receive Lamb waves in a variety of strain environments would help understand how the PZTs will degrade over time. Also a study of loads experienced by the aircraft parts identified for SHM (i.e. the F-15 bulkhead) is need to establish the range of strain experienced in the part. This thesis touches on the possibility of mode isolation, both with dual excitation and dual reception, more work with mode isolation could be used to minimize the effects the reflected waves, and thus minimize the impact of restricted geometry. Research should also include the effect of refracted Lamb wave energy around crack tips and its effects on measured response amplitude.

One potential source of error in this thesis is the disbondment of the PZTs. Research studying the output of other types of adhesives under the same loading conditions would be useful to understanding the behavior of the PZT as it is interacts with the material. As well, other materials should be used in PZT experiments. Before PZTs are attached to an F-15 bulkhead for SHM, experiments should show the actual behavior in the material of an F-15 bulkhead. Further research would also need to be conducted on an actual F-15. Static ground tests, ground tests with the engines running, and flight tests should be conducted to evaluate the performance of PZTs in a real environment.

Additionally, more efforts could be put towards confirming the conclusions of this research. Only two test plates were successful cracked, and more successfully crack test plates would increase the database of information from which to draw conclusions from. It would also help remove possible sources of error, such as delamination during one particular test.

This thesis examined Lamb waves traveling through the material to detect damage, future research should use surface (Rayleigh) waves instead of Lamb waves to detect damage. Surface waves behavior similarly to Lamb waves, but could have benefits to operating in the restricted geometry of an aircraft bulkhead.

Bibliography

1. "Basic Principles of Eddy Current Inspection". Available at http:// www.ndt-ed.org/ EducationResources/ CommunityCollege/ EddyCurrents/ Introduction/ IntroductiontoET.htm.

2. "Modes of Sound Wave Propagation". Online. Available at http:// www.ndt-ed.org/ EducationResources/ CommunityCollege/ Ultrasonics/ Physics/ mode-propagation.htm.

3. "Piezoelectric Theory and Applications". Catalog No.: 90-1015,. Available at http:// www.americanpiezo.com/ piezo theory/ index.html.

4. "NDI Methods", January 2008. Available at https://wwwmil.tinker.af.mil/ndi/.

5. Adams, Douglas E. *Health Monitoring of Structural Materials and Components.* John Wiley & Sons, Inc., The Atrium, Southern Gate, Chichester, West Sussex PO19 8SQ, England, 2007.

6. Andrews, Jennifer P. *Lamb Wave Propagation in Varying Thermal Environments.* Master's thesis, Graduate School of Engineering, Air Force Institute of Technology (AETC), Wright-Patterson AFB OH, March 2007. AFIT/GA/ENY/07-M01.

7. Crider II, Jeffrey S. *Damage Detection Using Lamb Waves for Structural Health Monitoring.* Master's thesis, Graduate School of Engineering, Air Force Institute of Technology (AETC), Wright-Patterson AFB OH, March 2007. AFIT/GA/ENY/07-M05.

8. Department of Defense. *Metallic Materials and Elements for Aerospace Structures.* Department of Defense Handbook, 2003.

9. Giurgiutiu, Victor. "Piezoelectric Wafer Active Sensor Embedded Ultrasonics in Beams and Plates". *Society for Experimental Mechanics*, 43(4):428–449, March 2003.

10. Giurgiutiu, Victor. "Tuned Lamb Wave Excitation and Detection with Piezoelectric Wafer Active Sensors for Structural Health Monitoring". *Journal of Intelligent Material Systems and Structures*, 16(291-305):57–65, April 2003.

11. Kusaka, T. and P. X. Qing. "Characterization of Loading Effects on the Performance of Smart Layer Embedded or Surface-Mounted on Structures". *Structural Health Monitoring 2003: From Diagnostics & Prognostics to Structural Health Management: Proceeding of the 4th International Workshop on Structural Health Monitoring.* Stanford, CA, November 2003.

12. Matthew S. Bond, James A. Rodriguez and Hieu T. Nguyen. *A Systems Engineering Process for an Integrated Structureal Health Monitoring System.* Master's thesis, Graduate School of Engineering, Air Force Institute of Technology (AETC), Wright-Patterson AFB OH, March 2007. AFIT/GSE/ENY/07-M02.

13. Saada, Adel S. *Elasticity Theory and Applications*. Krieger Publishing Company, Malabar, FL, 1993.

14. Steven E. Olson, Mark M. Derriso, Martin P. DiSimio. *Proceedings of the Third European Workshop*.

15. Swenson, Eric D. and Jeffrey S. Crider II. "Damage Detection Using Lamb Waves for Structural Health Monitoring". *6th International Workshop on Structural Health Monitoring*. Stanford, CA, September 2007.

16. Viktorov, Igor Aleksandrovich. *Rayleigh and Lamb Waves*. Plenum Press, New York, NY, 1967.

Vita

Captain Roman T. Underwood was born in Indiana and graduated from Kokomo High School in 1998. He attend Tri-State University from August 1998 to May 2002, when he graduated with a Bachelor of Science degree in Mechanical Engineering. He was accepted in the US Air Force Officer Training School in January 2003, and received his commission in April 2003. After commissioning Capt Underwood served as a Developmental Test engineer for the A-10, F-16, and UH-1N aircraft accumulating 73.9 flight hours. While at AFIT, Capt Underwood studied Finite Element Analysis and Structural Materials in the Aeronautical Engineering Department. Following graduation, he is assigned to the AFRL Nondestructive Inspection Field Office, Tinker AFB, OK.

Permanent address: 2950 Hobson Way
Air Force Institute of Technology
Wright-Patterson AFB, OH 45433

1. REPORT DATE (DD–MM–YYYY)	2. REPORT TYPE	3. DATES COVERED (From — To)
27-03-2008	Master's Thesis	Jan 2007 — Mar 2008

4. TITLE AND SUBTITLE	5a. CONTRACT NUMBER
Damage Detection Analysis Using Lamb Waves in Restricted Geometry for Aerospace Applications	5b. GRANT NUMBER
	5c. PROGRAM ELEMENT NUMBER

6. AUTHOR(S)	5d. PROJECT NUMBER
Roman T. Underwood, Capt, USAF	5e. TASK NUMBER
	5f. WORK UNIT NUMBER

7. PERFORMING ORGANIZATION NAME(S) AND ADDRESS(ES)	8. PERFORMING ORGANIZATION REPORT NUMBER
Air Force Institute of Technology Graduate School of Engineering and Management (AFIT/EN) 2950 Hobson Way WPAFB OH 45433-7765	AFIT/GA/ENY/08-M29

9. SPONSORING / MONITORING AGENCY NAME(S) AND ADDRESS(ES) :	10. SPONSOR/MONITOR'S ACRONYM(S)
DAGSI/AFRL 3155 Research Blvd, Suite 205 Kettering, OH 45420	11. SPONSOR/MONITOR'S REPORT NUMBER(S)

12. DISTRIBUTION / AVAILABILITY STATEMENT

APPROVED FOR PUBLIC RELEASE; DISTRIBUTION UNLIMITED

13. SUPPLEMENTARY NOTES

14. ABSTRACT

A goal of structural health monitoring (SHM) is to increase aircraft readiness through condition based maintenance (i.e. servicing an aircraft only when it is known to be necessary). The lead ziconate titanate (PZT) is a commonly used piezoelectric transducer that has shown potential to detect damage in aircraft structures without time consuming manual inspections. But many locations identified by the USAF for SHM have restricted geometries, presenting difficulties using the PZT transducers successfully. One known fatigue location in an aircraft bulkhead has been selected as a basis to evaluate some of the challenges of using PZT transducers for SHM. The goal of this research is use analytical and experimental investigations to detect fatigue cracks in plates representing the restricted geometry of the aircraft bulkhead. This research shows that detecting closed fatigue cracks can be more challenging than detecting open cracks, but that opening the cracks using an applied static load presents new challenges.

15. SUBJECT TERMS

Piezoelectric, Lamb waves, damage detection, fatigue crack

16. SECURITY CLASSIFICATION OF:			17. LIMITATION OF ABSTRACT	18. NUMBER OF PAGES	19a. NAME OF RESPONSIBLE PERSON
a. REPORT	b. ABSTRACT	c. THIS PAGE	UU	83	Dr. Som R. Soni
U	U	U			19b. TELEPHONE NUMBER (Include Area Code) (937) 255-3636, ext 3420; e-mail: Som.soni@afit.edu